Meteor shower modeling: Past and future Draconid outbursts

A. Egal[a,b,c,*], P. Wiegert[a,b], P.G. Brown[a,b], D.E. Moser[d], M. Campbell-Brown[a,b], A. Moorhead[e], S. Ehlert[f], N. Moticska[e,g]

[a] Department of Physics and Astronomy, The University of Western Ontario, London, Ontario N6A 3K7, Canada
[b] Centre for Planetary Science and Exploration, The University of Western Ontario, London, Ontario N6A 5B8, Canada
[c] IMCCE, Observatoire de Paris, PSL Research University, CNRS, Sorbonne Universités, UPMC Univ. Paris 06, Univ. Lille
[d] Jacobs Space Exploration Group, NASA Meteoroid Environment Office, Marshall Space Flight Center, Huntsville, AL 35812, USA
[e] NASA Meteoroid Environment Office, Marshall Space Flight Center, Huntsville, AL 35812, USA
[f] Qualis Corporation, Jacobs Space Exploration Group, NASA Meteoroid Environment Office, Marshall Space Flight Center, Huntsville, AL 35812, USA
[g] Embry-Riddle Aeronautical Univeristy, Daytona Beach, FL, USA

ABSTRACT

This work presents numerical simulations of meteoroid streams released by comet 21P/Giacobini-Zinner over the period 1850–2030. The initial methodology, based on Vaubaillon et al. (2005), has been updated and modified to account for the evolution of the comet's dust production along its orbit. The peak time, intensity, and duration of the shower were assessed using simulated activity profiles that are calibrated to match observations of historic Draconid outbursts. The characteristics of all the main apparitions of the shower are reproduced, with a peak time accuracy of half an hour and an intensity estimate correct to within a factor of 2 (visual showers) or 3 (radio outbursts). Our model also revealed the existence of a previously unreported strong radio outburst on October 9, 1999, that has since been confirmed by archival radar measurements. The first results of the model, presented in Egal et al. (2018), provided one of the best predictions of the recent 2018 outburst. Three future radio outbursts are predicted in the next decade, in 2019, 2025 and 2029. The strongest activity is expected in 2025 when the Earth encounters the young 2012 trail. Because of the dynamical uncertainties associated with comet 21P's orbital evolution between the 1959 and 1965 apparitions, observations of the 2019 radio outburst would be particularly helpful to improve the confidence of subsequent forecasts.

1. Introduction

The October Draconid shower (009 DRA) is an autumnal meteor shower known to episodically appear around the 9th of October since 1926. The Draconid shower, with apparitions irregular in time and intensity, has challenged the forecasts of modelers since its discovery. Its parent body is the Jupiter-family comet 21P/Giacobini-Zinner, discovered in 1900, which has an erratic and highly perturbed orbit (Marsden and Sekanina, 1971). The Draconid annual activity is usually barely perceptible (with a rate of a few visual meteors per hour), but the stream occasionally produces strong outbursts and storms (up to 10,000 meteors per hour) that are not directly correlated with the past geometrical configuration between the Earth and the parent comet (Egal et al., 2018). In addition, some showers were observed by naked-eye witnesses or using video devices, while other outbursts (e.g. 2012) were caused by small meteoroids only detectable by radar instruments (Ye et al., 2014).

Previous attempts to predict upcoming Draconid activity have had mixed success. Of the nine historic outbursts of the shower (1926, 1933, 1946, 1952, 1985, 1998, 2005, 2011 and 2012), five were expected (1926, 1946, 1985, 1998 and 2011) and predictions of three events correctly estimated the peak time with an accuracy better than 2 h. In 1946, the maximum activity occurred close to the descending node of the comet, simplifying timing estimates. (Reznikov, 1993) accurately predicted the shower return in 1998, caused by an encounter with the meteoroid stream ejected in 1926. More recently, a successful peak time prediction concerned the 2011 outburst. Numerical simulations of meteoroid streams ejected from 21P conducted by different authors estimated a maximum activity around 20h UT and a secondary peak around 17h on October 8, 2011 (Vaubaillon et al., 2011; Watanabe and Sato, 2008); the existence of both peaks was indeed confirmed by independent observation campaigns (e.g. Kac, 2015; McBeath, 2012; Trigo-Rodríguez et al., 2013).

If different models provided an accurate prediction of the 2011

---

apparition date, they also led to the first reasonable estimate of the outburst's strength. The activity of a shower, usually characterized by the zenithal hourly rate (ZHR) parameter (i.e. the number of meteors a single observer would see during an hour under ideal conditions), is a quantity that is hard to foresee. To our knowledge, no real intensity predictions were performed for Draconid outbursts prior to the 1998 apparition. The first attempt of Kresák (1993) to estimate the strength of the shower outburst in 1998, expected to be lower than the one occurring in 1985, underestimated the 1998 shower's intensity by a factor of ten.

In 2011, ZHR estimates of the main peak ranged from 40 to 50 (Maslov, 2011) to 600 (Vaubaillon et al., 2011; Watanabe and Sato, 2008), with intermediate activity predictions reaching storm level (ZHR of 7000 in Sigismondi, 2011). Numerous observations of the 2011 Draconids estimated a ZHR between 300 (Kero et al., 2012; McBeath, 2012) and 400–460 (Kac, 2015; Trigo-Rodríguez et al., 2013). Among the wide range of ZHR predictions for 2011 published in the literature, some were in good agreement with the observations (Vaubaillon et al., 2011; Watanabe and Sato, 2008). This success could have settled the question of Draconid forecasts using numerical simulations. However, a completely unexpected radio storm reaching a ZHR of 9000 ± 1000 meteors per hour was observed one year later (Ye et al., 2014), highlighting the need to improve the intensity predictions of meteor showers.

The motivation underlying the present work was therefore to be able to predict not only the date and time of appearance of a Draconid shower, but to also provide a quantitative estimate of its intensity with relative confidence. Since the numerical modeling of meteoroid streams ejected from the parent comet is the only efficient tool to predict such a shower, we performed simulations of the {21P, Draconid} complex using the model of Vaubaillon et al. (2005). For the first time, we simulated ZHR profiles for each year of predicted enhanced Draconid activity and compared them with the available observations. The simulated profiles were then calibrated against observations of the timing, activity profile and strength of historic Draconid outbursts to reinforce the reliability of future forecasts. This work presents the implementation and results of our meteoroid stream modeling, applied specifically to the Draconid shower. The structure of the paper is comprised of four main parts, some of which consist of multiple sections.

- In Section 2, we detail the main characteristics of the historic Draconid outbursts observed between 1926 and 2012. Because the Draconids were widely analyzed by multiple observers using different instruments, the literature has a wide variety of information relating to the shower. For each event, we tried to highlight the conclusions shared by the highest number of authors or the best documented reports.
- Sections 3, 4 and 5, together with Appendices A, B & C, describe in detail the implementation and interpretation of the new meteoroid stream model used here to reproduce or predict past and future Draconid occurrences (Model I). In Section 6, we offer a succinct summary of the independently developed NASA Meteoroid Environment Office's MSFC meteoroid stream model, used to validate Model I.
- Section 7 presents the performance of Model I in reproducing the main visual and radio outbursts observed between 1933 and 2012, in terms of years of appearance and shower time, strength, and duration. A comparison between our simulations and observations of the previously unreported 1999 radio outburst, revealed by our model, is also presented. An initial comparison between the 2018 prediction performed in Egal et al. (2018) and preliminary visual and radio observations of this recent outburst, shared by the International Meteor Organization (IMO), is given in Section 8. The simulated activity profiles presented in these sections form the main validation of the approach employed by Model I.

- Finally, Section 9 details our predictions for three potential radio outbursts expected in the next decade (2019, 2025 and 2029). The reliability of this forecast, intrinsically correlated to Model I's accuracy, is discussed in Section 10.

2. Draconid observations

The Draconids are known to have produced two storms observed optically in 1933 and 1946, as well as more moderate shower outbursts in 1926, 1998, and 2011. Other Draconid outbursts were detected mainly by radar techniques in 1952, 1985, and 2005, in addition to a radio storm in 2012. Very low activity from the shower was reported in 1972 instead of the intense outburst/storm that was originally predicted (Hughes and Thompson, 1973; McIntosh, 1972).

In this work, we classify the Draconid apparitions into three categories: the outbursts which were visually observed or recorded using optical instruments ("visual outbursts"), the showers mainly observed by radio/radar devices ("radio outbursts"), and weak or poorly documented showers.

2.1. Established visual outbursts

2.1.1. 1933
The 1933 storm occurred on October 9 around 20h15 UT (Watson Jr., 1934), for a total duration of about 4h30 (R. Forbes-Bentley in Olivier, 1946). ZHR estimates of the shower are very disparate and vary from around 5400 (Watson Jr., 1934) to 10,000 (Jenniskens, 1995) and even 30,000 (Cook, 1973; Olivier, 1946).

2.1.2. 1946
The 1946 storm was by visual, photographic, and radar techniques mainly in Europe and North America. The shower peaked around 3h 40–3h 50 UT on October 10, and lasted 3 to 4 h (Kresak and Slancikova, 1975; Lovell et al., 1947). Again, ZHR estimates in the literature vary between 2000 (Hutcherson, 1946) and 6800 (Kresak and Slancikova, 1975) or 10,000 (Jenniskens, 1995).

2.1.3. 1998
The 1998 outburst appeared on October 8, peaking around 13h10 UT (Arlt, 1998; Koseki et al., 1998; Watanabe et al., 1999) although (Šimek and Pecina, 1999) indicated a maximum around 13h35 UT. The total duration was about 4 h (Watanabe et al., 1999), and the maximum ZHR reached 700 to 1000 meteors per hour (Arlt, 1998; Koseki et al., 1998; Watanabe et al., 1999).

2.1.4. 2011
Following the concordant predictions of an outburst in 2011, the Draconids were observed on October 8 by many teams with many different observational techniques (radar, video, photography, visual). The main peak occurred around 20h–20h15 UT, for a total duration of about 3 to 4 h and a maximum ZHR estimate varying from 300–400 to 560 (Kac, 2015; Kero et al., 2012; Koten et al., 2014; McBeath, 2012; Molau and Barentsen, 2014; Toth et al., 2012; Trigo-Rodríguez et al., 2013).

2.2. Established radio outbursts

2.2.1. 1985
The 1985 peak occurred on October 8 between 9h25 and 9h50 (Chebotarev and Simek, 1987; Simek, 1994), probably around 9h35 UT (Lindblad, 1987; Sidorov et al., 1994). The observed shower duration varies from 3h (Lindblad, 1987; Mason, 1986) to 4h30 (Sidorov et al., 1994). An equivalent ZHR is estimated to be from around 400–500 (Lindblad, 1987; Simek, 1994) to possibly as high as 2200 (Mason, 1986). In agreement with the radio measurements, visual observations carried out in Japan in 1985 confirmed a ZHR higher than 500 shortly

before 10h UT on October 8 (Koseki, 1990).

2.2.2. 2005

The unexpected 2005 radio outburst was detected on October 8 around 16h05 UT (Campbell-Brown et al., 2006). The end of the shower was missed by radar, while the beginning was not observed using visual techniques (Koten et al., 2007); producing only a lower limit of 3 h for the shower duration. The equivalent ZHR was estimated to be around 150 (Campbell-Brown et al., 2006).

2.2.3. 2012

The 2012 storm happened on October 8 at 16h40, for a peak duration of about 2 h and an equivalent ZHR of 9000 (Ye et al., 2014). (Fujiwara et al., 2016) measured a total duration of the shower of about 3 h, with a peak time occurring between 16h20 and 17h40 UT.

2.3. Weak or controversial shower returns

2.3.1. 1926

The meteor activity observed by visual observers in October 1926 allowed the shower to be linked to comet 21P/Giacobini-Zinner. From 36 meteors observed between 20h20 and 23h20 (G.M.T.) on October 9, 1926, a ZHR of about 20 meters per hour was estimated (Denning, 1927). A Draconid fireball, observed around 22h 16 (G.M.T.) that night, impressed the observers by leaving a persisting train during half an hour (Denning, 1927; Fisher, 1934).

2.3.2. 1952/1953

Draconid activity was noticed by the Jodrell Bank radar on October 9, 1952, with a maximum ZHR of 170–180 around 15h40–50 min UT (Davies and Lovell, 1955). The shower duration was approximately 3 h. The apparition of Draconid meteors the following year, in 1953, is controversial; no enhanced activity was detected by the Jodrell Bank radar at any time within 12 h of the expected maximum time (Jodrell Bank, 1953), while other authors suggest some weak activity (Jenniskens, 2006).

2.3.3. 1972

Due to the favorable geometrical configuration between the comet and the Earth, a potentially strong outburst/storm was expected on October 8, 1972. However, no significant activity was observed (Millman, 1973). Radar observations revealed a diffuse component of the shower, with a weak maximum activity at October 8.2 ± 0.3 (Hughes and Thompson, 1973). Radio observations carried in Japan might however argue for a stronger radio activity, with a peak of 84 meters detected in a 10 min interval around 16h10 UT on October 8, 1972 (Marsden, 1972).

Having summarized the major observational features of the Draconids over the last century, our next goal is to reproduce the years of recorded activity, shower timing, strength and activity profile from a model. We attempt to do this employing a model with the fewest number of tunable parameters which also provides good fits to the most robustly determined characteristics of the shower.

3. Model I — simulations

3.1. 21P/Giacobini-Zinner

Comet 21P/Giacobini-Zinner was observed for the first time by M. Giacobini in 1900, and identified again by E. Zinner in 1913. Since its discovery, at least 16 apparitions of the comet have been observed and numerous orbital solutions produced. 21P is a typical Jupiter-family comet (JFC), with a period of approximately 6.5 years and a current perihelion distance of 1.03 au. The comet has suffered multiple close encounters with Jupiter through its history, resulting in our simulations in a global reduction of its semi-major axis and increase of its

eccentricity in 400 years. The comet's motion has also been affected by sudden and significant variations in the nongravitational forces (NGF) induced by its outgassing, causing 21P to be classified as an "erratic" comet (Sekanina, 1993). A particular discontinuity in the transverse NGF coefficient between 1959 and 1965 dramatically modified 21P's orbit (Yeomans and Chodas, 1989). The gas and dust production of the comet used to peak after perihelion before this epoch, while the maximum outgassing has occurred pre-perihelion since then (Blaauw et al., 2014; Sekanina, 1985).

3.1.1. Ephemeris

Several studies have tried to reproduce the comet's dynamical evolution during the 20th century, in particular a significant discontinuity in its orbital evolution observed between 1959 and 1965. Despite a moderately close approach with Jupiter in 1958, the gravitational influence of the giant planet did not seem to be responsible for the orbital variations observed around 1959 (Yeomans, 1971; Yeomans, 1972).

(Królikowska et al., 2001; Sekanina, 1985) were able to explain the NGF evolution of 21P by considering the precession of the comet's spin axis. However, Sekanina's model yielded unrealistic values of the comet's oblateness and rotation period (Królikowska et al., 2001; Yeomans, 1986), while the Królikowska analysis required many additional parameters derived from observations (e.g. relative times between the maximum activity and the perihelion passage for different apparitions) to correctly link all the comet's apparitions. Another independent explanation for the erratic orbital evolution of 21P could be the activation of discrete source regions at the surface of the comet, at specific locations and for a certain duration (Sekanina, 1993).

In their current state, neither of these models permits the comet's ephemeris to be reproduced without involving a detailed knowledge of its past apparitions; for our study, we therefore decided to rely directly on the observations. The comet's motion at each apparition is integrated from an orbital solution provided by the JPL Small Body Data Center,[1] with an external time step of 1 day and considering the asymmetric non-gravitational forces model of (Yeomans and Chodas, 1989).

3.1.2. Integration period

Because of the 1959 orbital evolution discontinuity, we chose to build the ephemeris of each apparition of the comet from the closest available orbital solution, and not from the most recent measured orbit of 21P. However, older observations of 21P (prior to 1966) were determined with less accuracy, which may reduce the reliability of our integrations. In order to evaluate the impact of this approach on the comet ephemeris, we compared the trajectories integrated from 15 distinct orbital solutions of 21P obtained for the years 1900, 1913, 1926, 1933, 1940, 1946, 1959, 1966, 1972, 1979, 1985, 1992, 1998, 2006, and 2013.

Fig. 1 illustrates the evolution with time of the minimum, maximum, and average similarity criterion D_{SH} (Southworth and Hawkins, 1963) for each pair of trajectories obtained (left panel). The middle panel presents the variations of the descending node's heliocentric distance for each initial orbital solution considered. The right panel was obtained by considering the same initial orbit (2006 solution) but integrating the trajectory with different nongravitational force models (no NGF, symmetric outgassing, and asymmetric outgassing, respectively).

In Fig. 1, we observe a slight increase of the D_{SH} around 1960. The D_{SH} evolution before this date coincides with the dispersion noticeable in the node distances plots. The first significant dispersion of the orbits occurs in 1898, as a consequence of a close encounter with Jupiter. Earlier close approaches with Jupiter in 1815 and 1732 also disperse the orbits. From this analysis, we conclude that the orbital solution

---

[1] https://ssd.jpl.nasa.gov/sbdb.cgi.
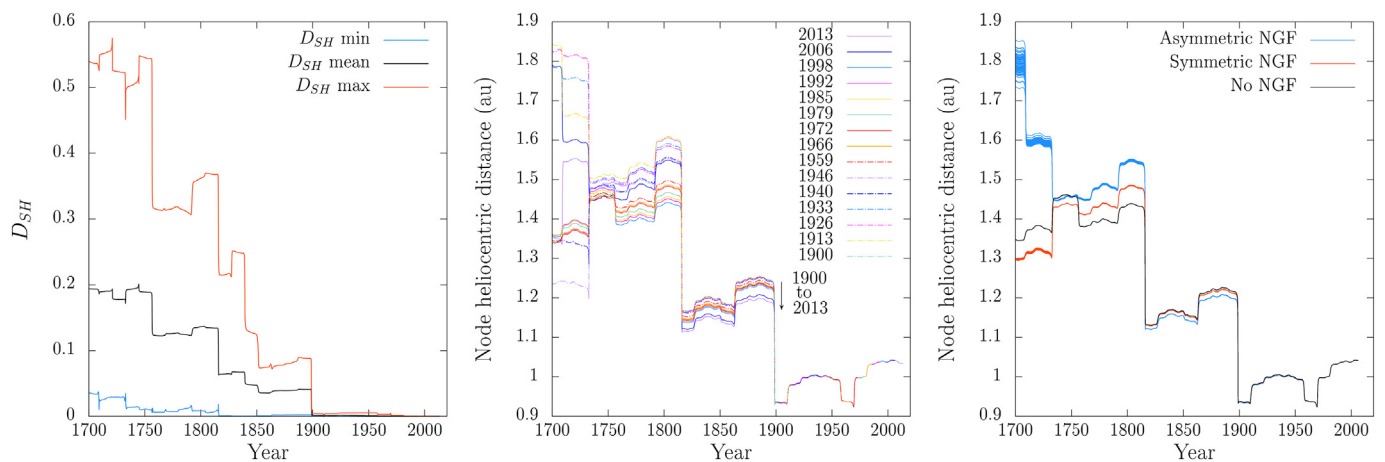
Fig. 1. Left panel: time evolution of the minimum, maximum, and mean D_{SH} between each pair of orbits determined from 15 distinct initial orbital solutions. Middle panel: heliocentric distance of the descending nodes of 21P along time, for 15 initial orbital solutions ranging from 1900 to 2013. Right panel: heliocentric distance of the descending node for different nongravitational forces models.

selected for the comet ephemeris computation should not influence the prediction of the meteor showers caused by trails ejected after the comet's discovery. For older streams, however, the initial integration epoch has a significant impact on the comet ephemeris, and hence on the meteoroid stream generated. Since the Draconids are often associated with young material (Lindblad, 1987; Vaubaillon et al., 2011; Wu and Williams, 1995), our integrations were limited to the 1850–2030 period. If any interpretation of the contribution of trails ejected prior to 1898 needs to be carefully conducted, their influence on our predictions is negligible. Particles ejected over the 1850–1898 period were only simulated for comparison of the nodal footprints of the simulated Draconids with previous works (e.g. with (Vaubaillon et al., 2011)).

3.1.3. Physical properties

The lack of direct imaging of 21P's nucleus forces us to estimate certain physical properties needed for our integrations. The radius of the nucleus of 21P is not well determined; estimates suggest it probably lies between 1 and 2 km (Lamy et al., 2004; Leibowitz and Brosch, 1986; Pittichová et al., 2008; Singh et al., 1997). By default, we consider a nucleus density of 400 kg m^{-3} and an albedo of 0.05 commonly assumed for JFCs (Hanner et al., 1992; Landaberry et al., 1991; Newburn and Spinrad, 1985). The percentage of active surface, unknown for 21P, is fixed to 20%. A summary of the model's parameters is presented in Table 1.

3.2. Meteoroid streams

3.2.1. Ejection

Particles are ejected at each simulation time step of the comet for heliocentric distances below 3.7 au (Pittichová et al., 2008). Around 12.48 million dust particles were simulated over the period 1850–2020, covering the size bins $[10^{-4}, 10^{-3}]$ m $(10^{-9}, 10^{-6})$ kg: (160,000 particles per apparition), $[10^{-3}, 10^{-2}]$ m $(10^{-6}, 10^{-3})$ kg: (190,000 particles) and $[10^{-2}, 10^{-1}]$ m $(10^{-3}, 1)$ kg: (130,000 particles). An additional sample of 120,000 particles in each size bin was ejected at each comet apparition between 1852 and 2025, and integrated until the year 2030 (9.72 million particles). In total, 22.2 million dust particles were simulated over the period 1850–2030.

The meteoroid density is assumed to be 300 kg m^{-3}, as determined by Draconid meteor observations (Borovička et al., 2007). Simulated particles are isotropically ejected from the sunlit hemisphere of the comet, with velocities determined by the (Crifo and Rodionov, 1997) model, which produces ejection speeds most in accord with recent in situ cometary measurements (c.f. A).

Table 1
Comet and meteoroid characteristics considered by Model I. See the text for more details.

Comet parameter	Choice	Reference
Shape	Spherical	
Diameter	2 km	Lamy et al. (2004)
Density	400 kg m^{-3}	
Albedo	0.05	
Active surface	20%	
Active below	3.7 au	Pittichová et al. (2008)
Variation index γ_1, γ_2	2.1, 7.3	This work
K_1	~ 100	This work
$Af\rho_{max}$	~1600–1800 cm	This work
Particle parameter	Choice	Reference
Shape	Spherical	
Size	10^{-4} to 10^{-1} m	
Density	300 kg m^{-3}	Borovička et al. (2007)
Ejection velocity model	"CNC" model	Crifo and Rodionov (1997)
Ejection rate	Each day	
N$_{particles}$/apparition	~ 840,000	

3.2.2. Integration

The stream integration is performed in Fortran 90 using a 15th order RADAU integrator with a precision control parameter LL of 12 (Everhart, 1985). The external integration step is fixed to one day and the internal time steps are variable, allowing close encounters with planets to be dealt accurately. The gravitational attraction of the Sun, the Moon, and the eight planets of the solar system as well as general relativistic corrections are taken into account. Solar radiation pressure and Poynting-Robertson drag are also included. The Yarkovsky-Radzievskii effect was neglected since the size of our simulated particles doesn't exceed 10 cm (Vokrouhlický and Farinella, 2000).

3.2.3. Impact selection

As a first selection, all particles that approach the Earth below a distance $\Delta X = V_r \Delta T$ are considered potential impactors, with V_r the relative velocity between the planet and the particle and ΔT a time parameter depending on the shower duration. The length of a typical Draconid shower doesn't exceed a few hours; we consider for this study a conservative time interval of $\Delta T = 1$ day and a distance threshold ΔX of 1.15×10^{-2} au. Potential impacting particles are, in a second step, individually integrated with a time step of one minute, in order to precisely estimate the date and position of their closest approach with the Earth.

4. Model I — interpretation

The primary goal of this work is to compare our simulated meteor showers to Draconid observations with the goal of matching the peak date, peak intensity, duration and overall activity profiles of past showers. Because of limited computational resources, the number of particles ejected in our model is not comparable to the true number of meteoroids effectively released by comet 21P/Giacobini-Zinner. It is therefore necessary to extrapolate from the comparatively finite number of simulated particles to the true number of particles in the stream.

Since the number of simulated particles that would physically impact the Earth is too small to derive a reliable flux profile, we consider each particle that passes within a sphere $\mathscr{S}$, centered on the Earth and with a given radius R_s, as contributing to the shower. The R_s value must be smaller than the previous ΔX spatial criterion to exclude surrounding streams not producing any activity at the Earth. On the other hand, R_s needs to be large enough to include a statistically useful sample of particles. The selection of the R_s parameters for the Draconids simulations is discussed in Section 4.2.

Once particles are selected using the reduced distance criterion R_s, we assign to each impactor a weight N_g which represents the scaling required to move from the small number of simulated meteoroids to the true number which would be released by the comet in the same ejection circumstances.

4.1. Weights

The weighting process implemented here relies mainly on Vaubaillon et al. (2005), with some differences. First, the evolution of the dust production for 21P/Giacobini-Zinner with the heliocentric distance r_h is extrapolated to each apparition from a photometric solution of the comet (cf. B). Second, the gas and dust production are not assumed to be proportional to each other; this decoupling allows the gas and dust production to evolve separately as a function of heliocentric distance (Sekanina, 1985). The main hypotheses underlying the weighting solutions are:

1. The nucleus is spherical, homogeneous and composed of dust and water ice.
2. The dust production of the comet, represented by the $Af\rho$ parameter (A'Hearn et al., 1984, cf. B), evolves with the heliocentric distance r_h. The gas-to-dust production ratio K is not constant over r_h.
3. The water molecules and the dust particles are ejected from the sunlit hemisphere of the nucleus, with an intensity varying with the angle θ from the subsolar point.
4. The size distribution of the particles follows a power law of index u.

Details of the weighting computation are provided in C. For a given apparition of the comet with a perihelion distance q, the number of particles ejected in all directions in the size bin $[a_1', a_2']$ during time Δt and around r_h is found to be:

$$\begin{cases} N_g = & K_2 \dfrac{J\Delta t}{2A(\Phi)} A_1(a_1', a_2') \cdot \left(K_1 \Delta r_h \dfrac{1}{2} \right. \\ & \left. - \dfrac{Af\rho_{max}}{\gamma ln(10)} \left[10^{-\gamma\left(r_h + \frac{\Delta r_h}{2} - q\right)} - 10^{-\gamma\left(r_h - \frac{\Delta r_h}{2} - q\right)} \right] \right) \\ \gamma = & \gamma_1 \text{ pre} - \text{perihelion and } \gamma = \gamma_2 \text{ post} - \text{perihelion} \end{cases}$$

(1)

where:

- K_2 is a tunable normalization coefficient constant over all the ejection conditions,
- $A(\Phi)$ is the nucleus albedo at phase angle Φ,
- $Af\rho_{max}$ is the maximum $Af\rho$ obtained for a given apparition (ejection

epoch),
- r_h is the meteoroid heliocentric distance at the time of ejection (in au),
- q is the perihelion distance (au),
- $A_1(a_1', a_2')$ is shorthand for $\int_{a_1'}^{a_2'} \frac{da}{a^u}$, with a the particle radius (in m),
- K_1 is a constant governing the $Af\rho = f(r_h)$ evolution (fit parameter),
- γ is the $Af\rho$ variation index, with $\gamma = \gamma_1$ for pre-perihelion locations and $\gamma = \gamma_2$ for post-perihelion measurements, and
- J is a function of the ejection velocity and the minimal and maximal particle radii that can be ejected from the comet (cf. C).

4.2. Flux and activity profile

The shower spatial number density $\mathscr{F}_s$ is estimated from the weighted number of particles entering the sphere $\mathscr{S}$ over time. In this work, the sphere radius is fixed to $R_s = V_\oplus \delta t$, with $V_\oplus$ the Earth's heliocentric velocity and δt a time parameter corresponding to the duration of the maximum activity of the shower. For the most intense Draconid outbursts (e.g. 1946), most of the activity was contained within a one-hour interval (Davies and Lovell, 1955; Kresak and Slancikova, 1975). For the main Draconid outbursts observed visually (1933, 1946, 1998 and 2011), we then choose $R_s = V_\oplus \times 1\,h$ ($R_s < 10$ Earth radii). When the total number of unweighted particles retained for the flux computation is lower than 15, δt is gradually increased until either the number of particles exceeds 15 or δt is 6 h (assumed to be the maximal duration of the shower). The flux $\mathscr{F}$ of meteoroids is obtained by:

$$\mathscr{F} = \mathscr{F}_s \cdot V_r$$

(2)

with V_r the relative velocity between the Earth and the meteoroid stream. The zenithal hourly rate of the shower is derived from $\mathscr{F}$ using (Koschack and Rendtel, 1990):

$$\text{ZHR} = \frac{\mathscr{A}_s \mathscr{F}}{(13.1r - 16.5)(r - 1.3)^{0.748}}$$

(3)

where r is the measured population index of the shower and $\mathscr{A}_s$ an observer's surface area of the atmosphere at the ablation altitude ($\mathscr{A}_s \sim 37{,}200\ \text{km}^2$).

4.3. Peak time estimate

The predicted peak date of the shower is determined by computing a weighted average of the simulated activity profile. The presence of additional peaks, as well as the intensity and the duration of the shower, are also derived from the ZHR evolution. In the case of simulated outbursts with a low number of particles retained for the flux computation ($\delta t > 1h$), the resolution of the activity profiles may compromise the validity of this approach. In such cases, the time of the peak maximum is taken to be the date of closest approach between the Earth and the median location of the meteoroid streams (Vaubaillon et al., 2005).

5. Model I — calibration

Before predicting any future Draconid showers, we need to determine the unknown parameters (K_2, u) of the weighting function in Eq. (1) which best reproduce the past observed outbursts. The results are particularly sensitive to the value of the size distribution index u of the meteoroids at ejection, since this value influences the intensity and the shape of the activity profiles as well as the peak time estimate.

The calibration is first performed on the four strong visual showers of 1933, 1946, 1998, and 2011 and then refined using the radio outbursts. The simulated ZHR profiles, derived from the meteoroid fluxes using Eq. (3) and a given population index r, are compared with the observations (see Fig. 4 later). We have chosen in the calibration

process not to allow a variable population index, but instead adopt a fixed value of $r = 2.6$ based on measurements of the 2011 (Kac, 2015; Toth et al., 2012) and potentially the 1933 shower (Plavec, 1957).

Our philosophy is that since any model can be improved when more free parameters are introduced, we chose to limit the number of tunable parameters to the absolute minimum required. In doing this, we decrease the match between the simulated and observed intensities of a specific shower in fixing r. However, this allows us to determine the weighting solution that best reproduces all the outbursts with minimum adjustable parameters, which we feel improves the robustness of the model shower prediction.

The best agreement between the simulated and the observed activity profiles for the four visual showers was obtained for an ejecta size distribution index u of 2.9. This value differs from our previous published estimate of 2.64 (Egal et al., 2018); differences between the two works are due to several factors. First, in this work, we have increased the number of simulated particles by 75% and used a slightly different weighting solution which better reflects the observed $Af\rho$ evolution of comet 21P. Second, the size distribution index used here was determined considering two additional outbursts (1999 and 2018), not included in Egal et al. (2018).

Our calibrated value of u lies in the range of measurements performed for 67P (drifting from 2 beyond 2 au to 3.7 at perihelion, cf. Fulle et al., 2016). The associated cumulative mass index ($s_{mc} = 0.63$ for $u = 2.9$) is somewhat lower than the value of 0.85 derived for comets 1P/Halley (McDonnell et al., 1987) and 81P/Wild 2 (Green et al., 2004). Unfortunately, no such in situ measurement has been performed for 21P. Indirect estimates of u, inferred by meteor observations, are hampered by the variability of the observed mass index changes with each apparition of the shower and even during an individual outburst (Koten et al., 2014). In addition, because the orbital evolution of a meteoroid is size-dependent, a fundamental difference between the size distribution index at the time of ejection and observation is not unexpected. Since no in situ or indirect measurement of this parameter has been performed for 21P, the value of $u = 2.9$ will be adopted through the rest of this study.

6. Model II — MSFC

For validation purposes, the Draconid streams simulated using Model I have been compared to an independent meteoroid modeling performed by the NASA Meteoroid Environment Office (MEO). The MEO's MSFC Meteoroid Stream Model, similar to the model presented above, is detailed in Moser and Cooke (2004, 2008). The position and velocity of 21P/Giacobini-Zinner is taken from the 2006 orbital solution and ephemeris provided by JPL HORIZONS.[2] The comet radius is assumed to be 1.7 km, i.e. an average of Churyumov and Rosenbush (1991), Landaberry et al. (1991) and Newburn and Spinrad (1989) measurements. 600,000 meteoroids are ejected at each apparition of the comet between 1594 and 2018, resulting in a total of about 35.4 million particles. Particles are released from the comet with a time step of 1 h, using the ejection model of Jones (1995) with a spherical cap angle of ejection of 30°. The size of the particles are distributed uniformly over log β, where $\bar{e}ta$ ranges from 10^{-5} to 10^{-2}. β is defined as the ratio between the forces due to the radiation pressure (F_{rad}) and the Sun's gravity (F_{grav}), and can be approximated by the following relation:

$$\beta = \frac{F_{rad}}{F_{grav}} \simeq \frac{5.7 \times 10^{-4}}{a\rho} \tag{4}$$

with a and ρ respectively the radius (m) and density (kg m^{-3}) of the particle. The selected β range of 10^{-5} to 10^{-2} corresponds to masses between 1 µg and 1 kg for the selected density of 1000 kg m^{-3}, and masses around ten times higher for the density of 300 kg m^{-3}

considered by Model I.

The meteoroid integration is performed exactly as described in Section 3.2.2. Particles are retained as potential impactors if they cross the Earth's orbital plane within 0.01 au of the planet, and within ± 7 days of the expected shower peak. The time and intensity of the shower's maximum activity are evaluated through computation of an impact parameter (IP), defined as

$$\text{IP} = \frac{R_\oplus + h_{atmos}}{D} \tag{5}$$

where $R_\oplus$ is the Earth's radius, h_{atmos} the height of the atmosphere, and D the Earth-particle distance at the time of nodal crossing. The impact parameter increases the weight of particles passing by the Earth more closely, and therefore more susceptible to contribute to a shower. A Lorentzian fit of the IP distribution as a function of the solar longitude allows the time of the shower peak to be estimated. The shower strength is usually estimated by scaling the IP distributions to historical observations (Table 2).

Since less time and effort was allocated for the analysis of the MSFC simulations, the output of Model I and Model II cannot be compared for all the shower's characteristics. Results of the MSFC model, successful in predicting previous Draconid outbursts (e.g. in 2011), are however presented in this work because they allow an assessment of the confidence level of the time and intensity predictions issued from Model I.

7. Outbursts post-prediction

The goal of this section is to investigate the agreement of our simulated activity profiles with historical observations of the Draconids in terms of peak time, peak intensity, and shower duration. In Section 7.1, the years of potential apparitions of the shower are appraised from the simulations. Details of each visual and radio outburst mentioned in Section 2 are detailed in Section 7.2.

7.1. Validation

7.1.1. Annual activity profile

Years of activity caused by particles of the three size bins simulated by model I are presented in Fig. 2. In this diagram, all the particles meeting the large distance criterion $\Delta X = 1.15 \times 10^{-2}$ au for Model I and below 0.01 au for Model II are included. The annual variation of the number of impactors presented in Fig. 2 is therefore not a good proxy for the shower's strength, but instead highlights the periods of potential activity.

From our simulations, we predict intense Draconid activity in 1933, 1946, 1998, and 2011 for particles with a size larger than 10^{-3} m (i.e., those visible to the naked eye). We also predict activity in 1940, which to our knowledge was not reported by any observer, as well as some in 1959, 2018, and around 1926. When considering smaller particles in the size bin $[10^{-4}, 10^{-3}]$ m, we see additional significant activity in 1953, 1972, 1985, 1999, 2012, and 2019, as well as minor contributions over the period 1985–2030 (including the 2005 outburst).

Both Model I and Model II were successful in reproducing all the years for which a Draconid shower was observed, except the 1952 radio outburst detected only by the Jodrell Bank radar (Jodrell Bank, 1953). For Model I, all the visual showers are clearly distinguishable in the profile while the faintest radio events are more complicated to identify (e.g. 2005). Fig. 2, shows that the models are good at reproducing the years of potential enhanced Draconid activity.

7.1.2. 1999 Outburst

Our model predicted strong activity rich in smaller particles on October 9 1,999, which would be detectable using radio instruments. This model outcome was robust and persisted despite several attempts (not detailed here) to change the weighting parameters and distance criteria to remove this seemingly non-shower outburst year while still

Table 2
Comet and meteoroid characteristics used by the MSFC model (Model II).

Comet parameter	Choice	Reference
Shape	Spherical	
Radius	1.7 km	See text
Active within	2.5 au	
Particle parameter	Choice	Reference
Shape	Spherical	
Size (β)	$\sim 10^{-5}$ to 10^{-2}	
Density	1000 kg m^{-3}	
Ejection velocity model		Jones (1995)
Cap angle	30°	
Ejection rate	Every hour	
$N_{particles}$/apparition	$\sim 600{,}000$	

the Draconids was found in the calibration data.

The radar echo data were processed to produce fluxes with the same single-station procedure as in Campbell-Brown et al. (2006), in which echoes occurring at 90° to the radiant are counted and background subtractions are applied. The collecting area of the radar was near maximum at the time of the observed shower, ranging from 500 to 750 km². The Draconid radiant was close to its lowest elevation of 50°. Approximately four hundred echoes occurred on the Draconid echo line in the 6 h surrounding the peak, compared to 30 sporadics the previous day. Fig. 3 presents the ZHR profile of the shower with time bins of 15 min. The peak activity occurred at 11h30 ± 15m, for an approximate ZHR of 1250 (assuming a mass index of 1.82, c.f. Pokorný and Brown, 2016). Unfortunately, no other radar dedicated to meteor observation and recording in October 1999 has been identified.
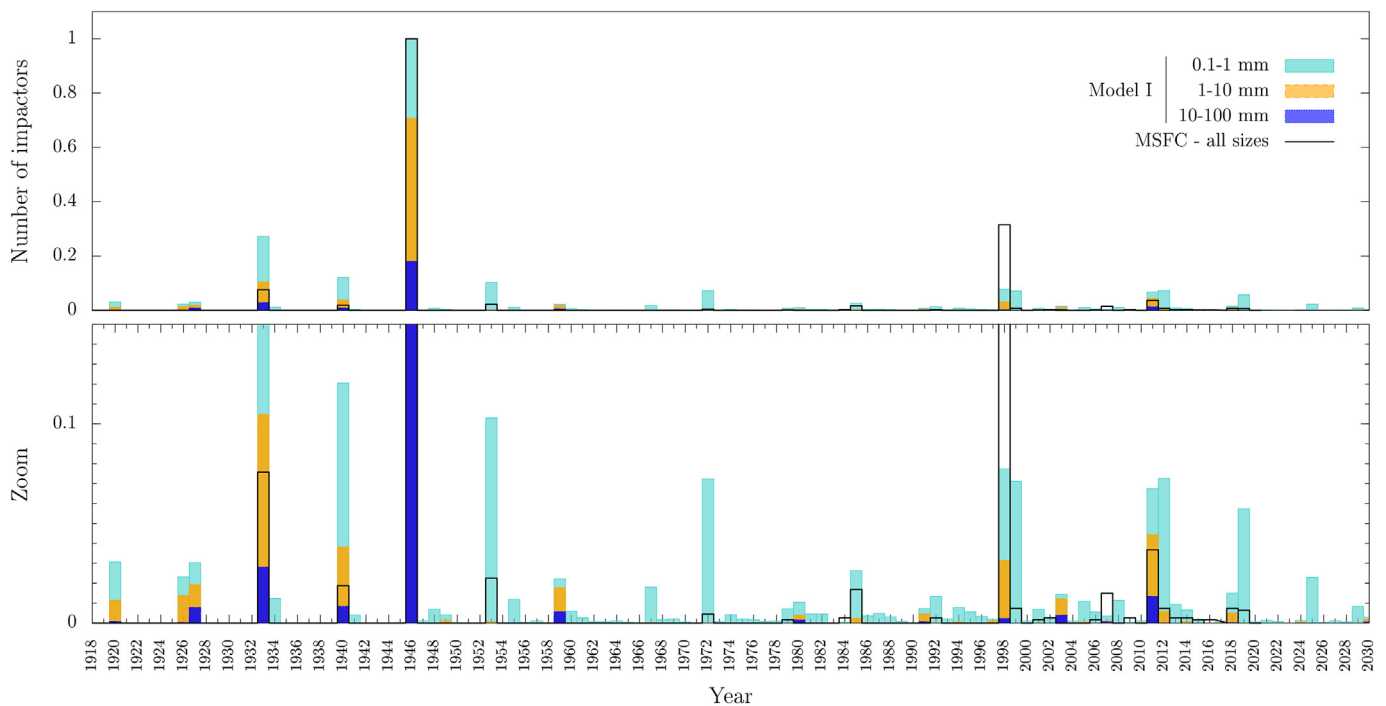
Fig. 2. The number of impactors (normalized to the number of particles in 1946) reaching the Earth over the period 1920–2030 for each size bin simulated by Model I (filled boxes) and for all the particles generated using Model II (bold line, MSFC model).

allowing fits to other years.

Few observations of Draconid activity in 1999 are recorded in the literature and no evidence for a strong radio shower was reported in the literature at the time. Some visual observations conducted from Europe on October 8 indicated low-level Draconid activity (Langbroek, 1999). Visual observations performed in Japan on October 9 also indicated a weak Draconid shower, with "a broad peak from 10h00m to 13h00m UT" and meteor rates small compared with those in 1998 (ZHR = 20–30, cf. Iiyama in Sato, 2003). These observations are consistent with the simulations, which predict intense activity of particles detectable by radar, but too small to be seen optically.

In 1999, (Brown et al., 2000) conducted a Leonid observation campaign in the Canadian Arctic (at Canadian Forces Station Alert, Nunavut) involving an automated meteor radar. The radar, an early version of the Canadian Meteor Orbit radar (CMOR), consisted of the 29 and 38 MHz systems, but lacked the outlying receivers needed for orbital calculations. It was located at 82.455°N, 62.497°W. Only the 29 MHz system was in operation on October 9, 1999 as part of early calibration prior to the Leonids; its transmitter power was 3.46 kW. Data from this calibration interval had been collected but not examined in detail prior to the current study, at which time a strong outburst from

Since our simulations allowed us to correctly reproduce the years of noticeable Draconid activity and provided a successful "prediction" of the 1999 radio outburst, we consider at this stage Model I to be validated. Next, we investigate each simulated shower in more depth.

7.2. Activity profiles

ZHR profiles derived for each year of activity are presented in Fig. 4. The first column of the figure groups the four main visual outbursts (1933, 1946, 1998, and 2011) and the second column the radio showers (1985, 1999, 2005, and 2012), whose characteristics are detailed below. The third column displays our simulations of the recent 2018 Draconids and of three potential future outbursts (in 2019, 2025 and 2029). These four cases are detailed in Sections 8 and 9.

When available, observed profiles (solid lines) have been superimposed on the simulation results (filled boxes). The maximum ZHR (number of meteors per hour) is compared here to the profile's maximum (using a time bin of 1 h for the model) while the peak time is estimated considering model time bins of 20 min. All the time estimates presented in this work have an accuracy of about half an hour. A summary of the main results shown in Fig. 4 is provided in Table 3.
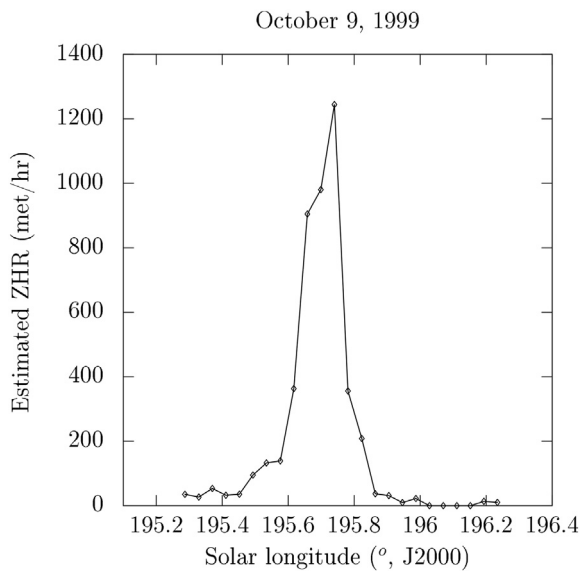
October 9, 1999

Fig. 3. Draconid ZHR profile determined from radar measurements performed at Alert on October 9, 1999, assuming a mass index of $s = 1.82$.

7.2.1. Established visual outbursts

7.2.1.1. 1933. From the modelled activity profile, we predict a maximum on October 9, around 20h13 ($L_\odot = 197.005°$), reaching a ZHR of 5830. The outburst is caused by particles ejected during the 1900 and 1907 apparitions, with a minor contribution from the 1886 and 1894 perihelion approaches. Most of the particles (71%) belong to the size bin $[10^{-3}, 10^{-2}]$ m, with a significant contribution of smaller particles (23% $\in [10^{-4}, 10^{-3}]$ m) and some large particles (5%). The simulated outburst duration is 5 h, consistent with the observations.

7.2.1.2. 1946. The simulated maximum occurs on October 10, around 3 h38 ($L_\odot = 196.986°$), reaching a ZHR of 7960. The outburst is caused by particles of several streams ejected between 1900 and 1940, with the largest contributions from the 1900 and 1907 trails. The vast majority of particles belong to the visible range, with a large number of particles having sizes between 10^{-2} and 10^{-1} m (65%). The total duration of the simulated outburst is 4h30, in good agreement with measurements. The predominance of the 1900 and 1907 trails influence on the 1933 and 1946 storms is consistent with the results of Reznikov (1993) and Vaubaillon et al. (2011).

7.2.1.3. 1998. The simulated activity peaks on October 8, around 13 h26 ($L_\odot = 195.087°$), reaching a ZHR of about 900. The outburst is caused by particles of the 1926 trail only, mainly with sizes in the ranges $[10^{-3}, 10^{-2}]$ m (67%) and $[10^{-4}, 10^{-3}]$ m (29%). The estimated shower duration is 4 h. Contrary to Sato (2003), we don't need to assume weak activity of the comet in 1926 to explain the intensity of the 1998 outburst compared to the 1933 and 1946 storms.

7.2.1.4. 2011. The modelled maximum activity occurs on October 8, around 20 h06 ($L_\odot = 195.033°$), reaching a ZHR of 550. The outburst is mainly caused by particles from the 1900 and 1907 streams, potentially leading to two maxima around 19h30 and 20h–20h15 (cf. Section 2). However, the resolution of the simulated profile of Fig. 4 does not permit reliable identification of the observed secondary peak. From our simulations, the outburst is mostly composed of particles of size $[10^{-3}, 10^{-2}]$ m (62%), with the remainder split evenly between smaller and larger particles. The estimated total duration of the shower is 4 h, consistent with observations.

7.2.2. Established radio outbursts

7.2.2.1. 1985. The simulated maximum occurs on October 8, around

9 h42 ($L_\odot = 195.260°$), reaching a ZHR of 370. The outburst is caused by the stream ejected in 1945, with a minor contribution from the 1933 apparition. Most of the particles contributing to the ZHR belong to the radio range ($\in [10^{-4}, 10^{-3}]$ m, 89%) with some candidates between 10^{-3} and 10^{-2} m (11%). No larger particles from the simulations were found to encounter the Earth. The total simulated duration (including all the activity detected and not only the central activity plateau) is slightly shorter than 9 h.

7.2.2.2. 1999. The simulated activity peaks on October 9, around 11 h13 ($L_\odot = 195.728°$), reaching a ZHR of 1380. The outburst is exclusively caused by small particles ($\in [10^{-4}, 10^{-3}]$ m, 100%) ejected in 1959 and 1966. For this simulated profile, we encountered an unusual situation. A small number of particles (< 10) belonging to the 1966 trail fulfilled all the ejection circumstances required to increase their weight (ejection at perihelion, low phase angle, very small size, etc.). This combination led to weights > 10 times higher than any other of the 22.7 million particles simulated. Taken at face value this would produce a maximum ZHR of about 50,000 meteors per hour. Given the exceptional nature of the ejection and excessive weighting compared to all other simulated particles, they were removed from the analysis as being unphysical and from the profile of Fig. 4. The total duration of the simulated outburst is about 6h45.

7.2.2.3. 2005. The 2005 profile represents the worst match between our simulations and the observations. In exploring matches, we consistently found that weighting parameters adopted which better reproduce this outburst, led to a general model solution which was poorer for all other shower return fits. Allowing this poor fit between the simulations and observations for the 2005 return we feel is justified by the low intensity of the shower and the reduced confidence in the time estimates derived from the observations (Campbell-Brown et al., 2006; Koten et al., 2007).

From the coarse simulated profile, we estimate a maximum activity on October 8, around 16h06 ($L_\odot = 195.401°$), reaching a ZHR of 50, composed only of particles in the radio range. Contrary to the simulations in Campbell-Brown et al. (2006), the best agreement with the observed time and intensity was found for particles ejected in 1953 and not 1946. Differences in the comet ephemeris might explain this divergence. For this poorly simulated profile, a maximum duration of 7 h is expected.

7.2.2.4. 2012. The simulated maximum occurs on October 8, around 16 h20 ($L_\odot = 195.610°$), reaching a ZHR of 3450. The outburst is only caused by small particles belonging to the 1966 stream. Similar to Ye et al. (2014), we find that the nodal footprint of the 1966 trail does not cross the Earth's trajectory (cf. Fig. 5). This might account for our underestimate of the shower's intensity; the 2012 outburst reached storm level with about 9000 meteors per hour. However, the particles reaching the planet's vicinity allow us to derive an activity profile that is consistent in time with the observations, with a total duration slightly shorter than 11 h.

7.2.3. Post-prediction summary

As a result of the calibration, each simulated profile of a visual outburst accurately matches the observations in terms of peak time (< 30 min) and maximum intensity (within a factor of 2, consistent with the uncertainties related to the meteor observations). The duration of the simulated profiles slightly exceeds the real duration of the shower, but still allows the period of noticeably enhanced activity to be constrained.

By applying the same weighting parameters to all observed showers, the simulated profiles are less able to reproduce details of the Draconid radio outbursts. Because of the lower number of small model particles reaching the Earth ($N_{part} \simeq 15$), all the radio profiles presented in this section have irregular shapes, with gaps in solar longitude that make
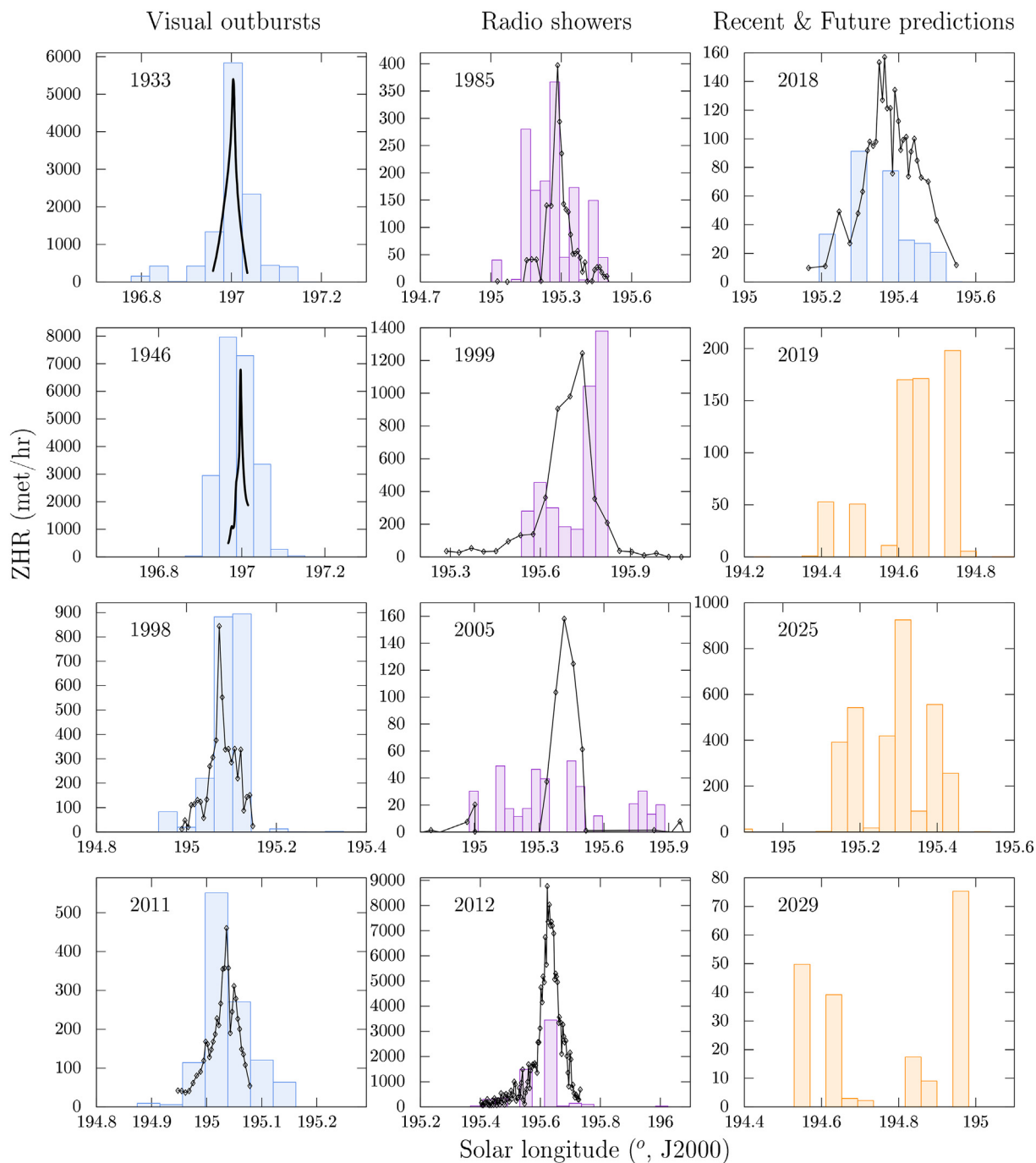
Fig. 4. Observed (black solid curve) and simulated (filled boxes) ZHR profiles of nine historic Draconid outbursts between 1933 and 2018 and predictions of three future occurrences of the shower. References for the observations are 1933: Watson Jr. (1934), 1946: Kresak and Slancikova (1975), 1998: Watanabe et al. (1999), 2011: Kac (2015), 1985: Mason (1986), 2005: Campbell-Brown et al. (2006), and 2012: Ye et al. (2014). The 1999 profile is compared to radar measurements performed in Alert (cf. Section 7.1.2) and the 2018 profile is compared with the ZHR derived from the IMO VMDB, accessed 15/12/2018. (For interpretation of the references to colour in this figure legend, the reader is referred to the web version of this article.)

their comparison to radar measurements difficult. However, both peak time estimates provided in Table 3 are consistent with the observed maximum activity with an error of less than half an hour. The shower strength, which is much more variable, matched the observations within a factor of 3 in the worst cases such as 2005 and 2012. Despite the apparent discrepancies between the shower duration reported in the literature and our simulations (e.g. in 1985), a quick look at Fig. 4 confirms that we correctly constrained the time window of most of the radio showers.

For the first time, to our knowledge, we have presented in this

section simulated ZHR profiles that allow us to quantitatively estimate the peak time, intensity, and duration of the main Draconid outbursts with reasonable accuracy.

8. Draconids 2018

8.1. Predictions

From the simulation of 12 million particles using Model I and a slightly different weighting scheme, we performed a prediction of the

Table 3

Summary of the observed (left panel) and simulated (right panel) characteristics of the historic Draconid outbursts. *Peak time estimated from the stream median location; see Section 4.3. [a]: reported full width at half maximum in 2018 (Molau, personal communication).

	Observations				Simulations					
					Model I				MSFC model	
Date (y/m/d)	Time (UT)	Reported duration	ZHR		Time (UT)	Total duration	ZHR	Time* (UT)	Time (UT)	ZHR
1933/10/09	20h15	4 h30	5400 to 30,000		20h13	5 h	5830	20h08	20h14	Strong
1946/10/10	3h40–50	3–4 h	2000 to 10,000		3h38	4 h30	7960	3h39	4h05	Storm
1985/10/08	9h25–50	4 h30	400 to 2200		9h42	8 h30	370	10h43	10h33	Outburst
1998/10/08	13h10	4 h	700 to 1000		13h26	4 h	900	13h22	13h19	Strong
1999/10/09	11h15–45	5 h	1250		11h13	6 h45	1380	11h30	11h57	Moderate
2005/10/08	16h05	≥3 h	150		16h06	7 h	50	16h28	Oct. 9, 3 h52	Weak
2011/10/08	20h00–15	3–4 h	300–400 to 560		20h06	4 h	550	20h03	19h48	Outburst
2012/10/08	16 h40	2 h	9000		16h20	10 h30	3450	15h58	16h42	Weak
2018/10/08	23 h15–45	3 h30[a]	100–150		22h51	8 h	90	23h45	0h30	Moderate

2018 Draconids in Egal et al. (2018). As found in several other studies, our work suggested that the Earth would cross the meteoroid stream through a gap between the 1946 and 1953 trails. The extremely small number of particles reaching the Earth's vicinity and retained for the flux computation in this orbital configuration prevented us from confidently predicting a complete simulated profile. The peak time was therefore estimated from the date of the closest approach to the stream median location (cf. Section 4.3). This approach, which we have found to be more robust in cases with low numbers of model particles, led to a maximum activity estimate around 23 h51 ($L_\odot = 195.390°$) on October 8, 2018. The model maximum ZHR profile being about 80 (with a factor 3 uncertainty), we had predicted an activity not exceeding a few tens of meteors per hour. However, our predictions at the L_1 and L_2 Lagrange points suggested storm-level activity at these locations, leading to the temporary re-orientation of the Gaia satellite (personal communication from Serpell, 2018).

The updated simulated profile for 2018, calibrated using the larger sample of about 22 million particles, is presented in Fig. 4. Compared to our previous work (Egal et al., 2018), we note a slight modification of the profile shape, but no significant variations of the maximum intensity (90 meteors per hour) or time (23h45 using the median location method, $L_\odot = 195.348°$). In our simulations, all the particles reaching Earth belong to the 1953 trail, and have relatively small sizes ([$10^{-3}, 10^{-2}$] m: 87%, [$10^{-4}, 10^{-3}$] m: 12%,). Almost no large particles encountered the Earth.

8.2. Observations

At the time of writing, no definitive measurements of the Draconids 2018 have been published. However, as a preliminary comparison with our predictions, the ZHR profiles issued from the International Meteor Organization Visual Meteor Database (IMO/VMDB)and the IMO Video Meteor Network (IMO/VMN)[3] were superimposed on the simulation results in Fig. 6. The black solid curves represent the original measurements, and the light boxes the data re-binned in time steps consistent with the simulated profile (dark boxes). We observe that the length of the simulated profile matches well both sets of observations and that the peak time estimate is accurate to within a half an hour of uncertainty (depending on when the maximum activity really occurred). The simulated intensity underestimates the real strength of the shower, but remains correct within a factor of 2. From these preliminary observations, we conclude that despite the low number of particles involved in the shower simulation, our model led to one of the best predictions of the 2018 Draconids published (Egal et al., 2018).

9. Future Draconid outbursts

Finally, in an effort to predict Draconid activity over the next decade, we integrated a sample of particles generated by Model I until the year 2030. In total, 360,000 particles equally spread over our three size bins ([$10^{-4}, 10^{-3}$] m, [$10^{-3}, 10^{-2}$] m and [$10^{-2}, 10^{-1}$] m) were ejected at each apparition of the comet from 1850 to 2030, resulting in a total of about 9.72 million simulated meteoroids. The model predicted overall peak intensity of the shower covering the period 2020–2030 is presented in Fig. 2.

From this annual variation in the predicted shower strength, we estimate enhanced radio activity in 2019 and 2025, as well as a potential minor display in 2029. Comparing to the predictions of other modelers, we observe that enhanced activity in 2019 and2025 is also predicted by Maslov (2011) and Ye et al. (2014). We however do not share the forecast of a low intensity shower in 2021 mentioned in Ye et al. (2014).

9.1. 2019

On October 82,019, the model predicted that the Earth will face a similar situation to that in 1999 and encounter the streams ejected by 21P in 1959 and 1966. Our estimated activity profile, presented in Fig. 4, is exclusively composed of particles in the size bin [$10^{-4}, 10^{-3}$] m. As with the radio outburst in 1999, a small number of unphysically heavy weighted particles belonging to the 1966 trail raised the ZHR maximum to a storm value of 5000 meteors per hour and have been removed from the analysis.

The low temporal resolution of the simulated profile, typical of our other simulated radio showers, decreases the precision of the time and intensity predictions compared to strong visual outbursts. We estimate, however, that the Earth might experience a radio outburst with a maximum ZHR of about 200 (within a factor of 3), and enhanced activity between 5h45 and 15h30 UT on October 8. The peak time is difficult to assess from the model profile. If the maximum ZHR is reached around 14h35 UT, ($L_\odot = 194.753°$), the weighted average of the profile has a peak time of 12 h UT ($L_\odot = 194.648°$). When considering the date of the closest approach between the Earth and the median location of a specific stream, we estimate a maximum activity caused by the 1959 stream around 13h42 UT ($L_\odot = 194.718°$) and a maximum caused by the 1966 stream at 12h01 UT. The total duration of the shower, among the longest for radio showers in our simulations, is 9h45.

Simulations performed by other authors differ from our predictions, either in time and intensity. Results from the MSFC model, differing from Model I mostly on the ejection circumstances and the weighting process, augurs for noticeable Draconid activity(nearly as strong as in
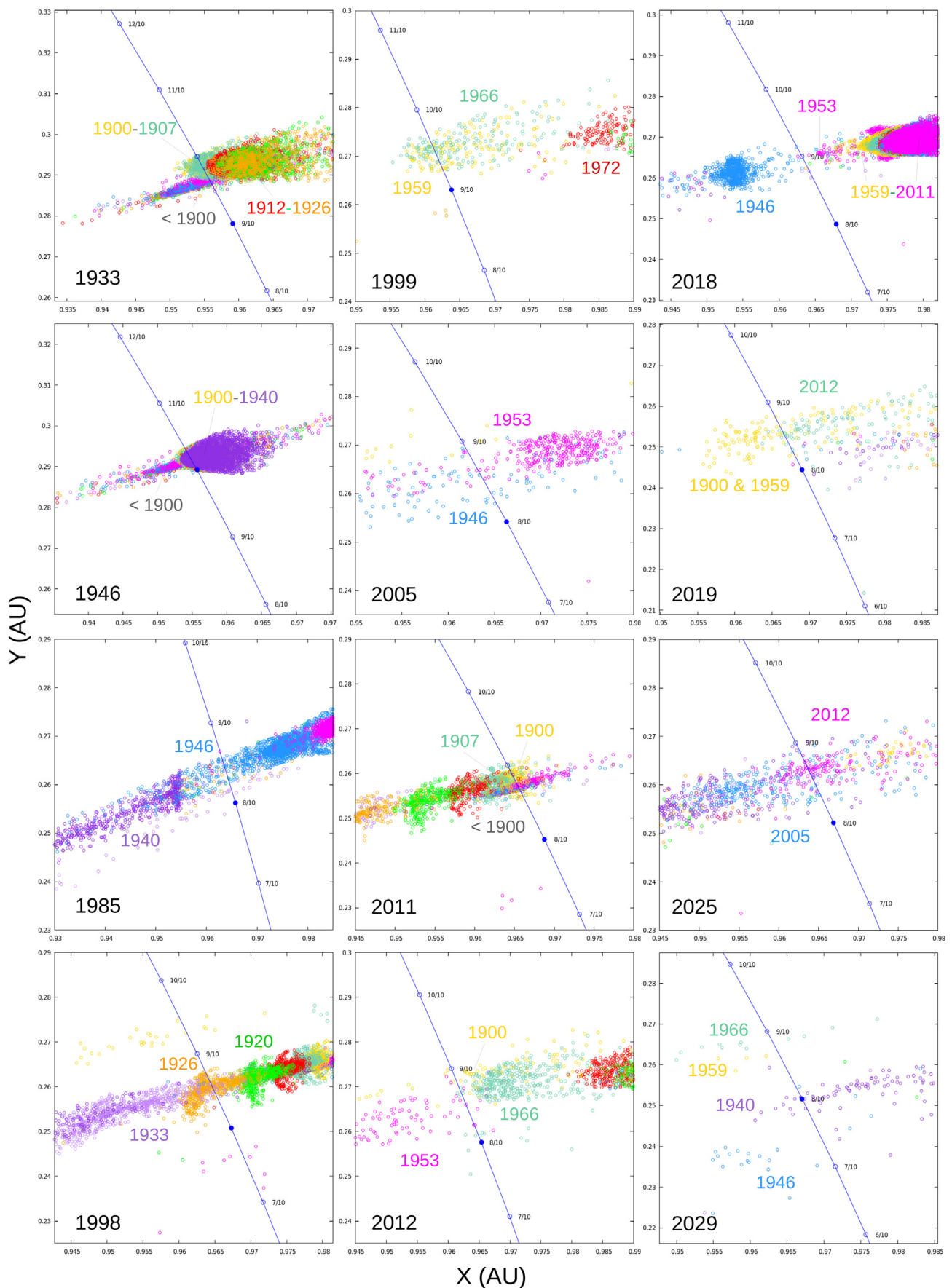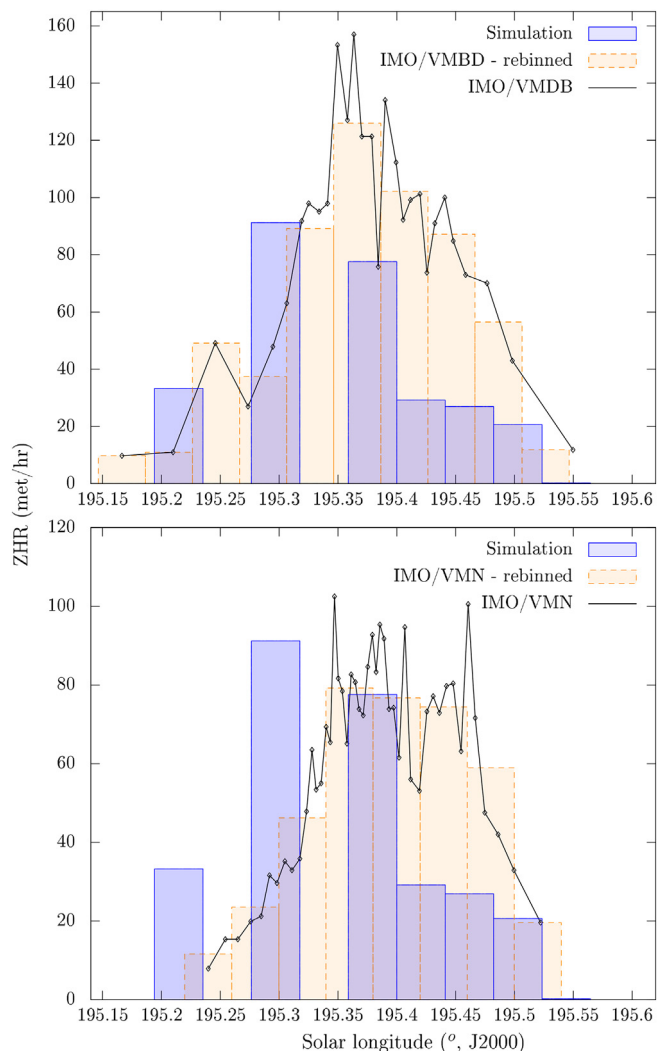
Fig. 5. Nodal footprint of the simulated Draconids crossing the ecliptic plane for years of predicted enhanced activity. The line connects the Earth's positions at the considered dates.

Fig. 6. Comparison between the 2018 simulated profile (dark boxes) and preliminary observations released by the International Meteor Organization. Visual observations are shown in the top panel & video observations in the bottom panel; the simulation results are identical in the two panels.

2018) culminating around 15h06 UT on October 8 ($L_\odot = 194.775°$) consisting of mainly smaller particles. A secondary peak might be expected much earlier, around 4h20 the same day ($L_\odot = 194.332°$). According to Maslov (2011), the activity level from the 1959 trail in 2019 should be about half of that in 1999. Based on the 1999 ZHR estimated by (Iiyama in Sato, 2003), Maslov expects "a small visual peak not higher than ZHR 5-10, on 2019 October 8 at 14h45m UT". He however points out that "radio observations could show much higher activity" (Maslov, 2011).

In Jenniskens (2006), no enhanced Draconid activity was predicted by J. Vaubaillon in 2019. However, some revised predictions are presented in Table 4. The first one points toward a potential storm on October 8, with a peak time consistent with the MSFC and Maslov's (2011) results. His ZHR estimate of about 4000 meteors per hour is also in agreement with our simulations when we do not remove the heavily weighted particles. The second prediction, favored by that author because it uses the more accurate ephemeris of the comet provided by JPL, indicates a moderate outburst on October 7 around 11h UT (Vaubaillon, personal communication).

In Kastinen and Kero (2017), no specific activity is discernible for 2019 compared to historic Draconid outbursts. Ye et al. (2014) attribute enhanced activity in 2019 to small particles belonging to the 1979 trail.

The maximum activity is expected to be lower than in 2018 and to peak around $L_\odot = 194.2°$ ($\in[194,195]°$).

A summary of the 2019 predictions is provided in Table 4. Different estimates of the shower's characteristics are highly variable and no general agreement about the peak time and intensity is found. When considering the weighted average of our simulated activity profile, the peak time is driven by the influence of the 1966 trail and the resulting prediction is in advance of 3 h compared to the MSFC or the Maslov (2011) results. The maximum of the ZHR distribution is consistent with these two models, but was not used in our model's validation. The expectations of the shower's strength are even more uncertain, and vary from a low activity (Kastinen and Kero, 2017; Maslov, 2011; Ye et al., 2014) to a radio outburst (this work, Model I and MSFC model).

9.2. 2025

In our simulations, the Earth crosses a portion of the meteoroid stream composed of small particles at the 2025 Draconid return mainly ejected during the 2011–2012 apparition, with some contribution from the 2005 and potentially the 1999 trails. From the activity profile, we estimate a maximum activity around 16h18 UT on October 8 ($L_\odot = 195.286$). The Earth is expected to approach the median location of the 2012 trail around 15h30 UT ($L_\odot = 195.252°$) and the 2005 trail at 13h40 UT ($L_\odot = 195.178°$). Our maximum intensity (✳3) reaches a ZHR of 950 meteors per hour.

According to Maslov (2011), encounters with the 1907 to 1953 trails will lead to multiple submaxima at 05h01 UT (ZHR: 10–15), 07h25 UT (ZHR: 20–25), 09h06 UT (ZHR: 20–25), and 10h17 to 10h49 UT (ZHR: 50–60), with many fireballs expected. Consistent with our prediction, Maslov (2011) also predicts an encounter with the 2012 trail on October 8, 2025 around 15h14 UT. If the expected visual activity is low (10–40 in ZHR), the author anticipates a much higher radio activity going up to tens of thousands of meteors per hour. Because both forecasts point toward a very strong radio outburst/storm caused by an encounter with the young (and therefore probably dense) 2012 trail, special attention should be paid to this event.

9.3. 2029

The 2029 ZHR profile and node plot (cf. Figs. 4 and 5) are hard to interpret. Only some particles (*Npart* < 10) ejected in 1940 approach the Earth in our simulations, leading to the low-resolution shape of Fig. 4. For this specific shower, more simulations of the 1940 trail in particular are needed. Our first impressions are that we might detect some weak radio activity the night between October 7 and 8, which was not predicted by Ye et al. (2014) or Maslov (2011).

10. Discussion

Numerical models of meteor showers are forced to rely on multiple assumptions. Each attempt to better reproduce the comet's behavior requires the incorporation of new parameters, which are usually not measured for the parent body in question. In this section, we address the influence that certain of our assumptions have on our forecasts of future Draconid outbursts.

10.1. Comet characteristics and ephemeris

As mentioned in Section 3.1, after one century of observations, comet 21P/Giacobini-Zinner remains a mysterious comet. Its physical characteristics are not well defined, and the accuracy of its ephemeris is poor prior to 1966 because of multiple close encounters with Jupiter and erratic variations in its nongravitational forces. A significant orbital discontinuity was observed in 1959–1965, changing the comet ejection patterns and orbital evolution. These considerations led us to adopt orbital solutions available for 21P based on observations at a particular

Table 4
2019 Draconid forecasts performed by independent modelers. Sources: (1) This work, (2) Moser (2018), (3) Personal comment, (4) Maslov (2011), (5) Ye et al. (2014).

Modeler	Trail	Date (y/m/d)	Hour	$L_\odot$	ZHR	Comment
Egal (1)	Mult.	2019/10/08	12h	194.648	200 ✳ 3	From the ZHR profile (main prediction)
	Mult.	2019/10/08	14h35	194.753	200 ✳ 3	Maximum of the ZHR profile
	1959	2019/10/08	13h42	194.718	–	Based on stream median location
	1966	2019/10/08	12h01	194.648	–	Based on stream median location
MSFC (2)	Mult.	2019/10/08	15h06	194.775	~ to 2018	Primary peak
	Mult.	2019/10/08	4h20	194.332	–	Secondary peak
Vaubaillon (3)	Mult.	2019/10/08	14h41	193.522	4042	Old comet ephemeris
	Mult.	2019/10/07	11h01	192.811	363	Updated comet ephemeris (recommended)
Maslov (4)	1959	2019/10/08	14h44	194.759	5–10 (visual)	Likely higher activity in radio range
Ye (5)	1979			194.2 ($\in$[194.0,194.5])		Lower rate than in 2018

apparition instead of computing its ephemeris backward in time from a precise and recent solution. This decision, forcing us to sometimes rely on less precise orbital measurements (but allowing us to take the 1959–1965 discontinuity into account), may explain the preponderance of different streams involved in our simulated 2005 and 2019 showers compared to other authors (Campbell-Brown et al., 2006; Ye et al., 2014). As noticed in Vaubaillon et al. (2011), the choice of the ephemeris solution has, therefore, an impact on the shower predictions.

By comparing the post-predictions performed using Model I and the MSFC model, which is similar in methodology but assumes different physical characteristics of the comet and ejection circumstances, we observe that both approaches provided consistent conclusions about the years of enhanced Draconid activity, the streams contributing to the shower, and the particles' characteristics (size and ejection velocity). We also notice that the peak time estimates of the historic Draconid outbursts predicted by Model I (from the profiles and the stream median location) and by the MSFC model are similar. We therefore consider the exact choice of the comet's physical parameters and the ejection circumstances to have only a moderate influence in the predictions of the existence and date of enhanced Draconid activity.

10.2. Weights and ZHR computation

The weighting solution for comet 21P, detailed in B and C, has an extremely significant impact on the shower's predicted level of activity. In this work, we have updated the weighting solution of Vaubaillon et al. (2005) considering pre- and post-perihelion dust measurements of comet 21P during the 2018 apparition. The heliocentric distance dependence of the amount of dust ejected by the comet was established from these observations and applied to all the previous apparitions considered in our model.

Despite the evident limitations of this approach, this solution offers a first approximation of the comet's behavior throughout its period of activity and has the merit of being based on real measurements of the comet's activity. Any further modification of 21P's $Af\rho = f(r_h)$ can also easily be implemented in the model to improve future shower predictions.

Among the unknown parameters of the weighting function 1, the most influential and uncertain one is the particle size distribution index at ejection, u. Coupled with the number of particles required to produce a ZHR profile (> 15) and the maximum sphere size adopted for the flux computation ($6h \times V_\oplus$), the value of u can substantially modify the shape, peak time, and intensity of the simulated profiles. It is therefore difficult to conclude that the profiles presented in Fig. 4 provide an accurate prediction of future Draconid outbursts. However, by calibrating these parameters to strong and well-known visual outbursts (cf. Section 5), their impact on the final prediction is reduced.

To illustrate this, we compare the conclusions of the present work with the previous analysis published in Egal et al. (2018). We observe that with a different weighting solution, a different size distribution index, a higher number of particles required for the profile computation

(15 instead of 10), and a larger sample of particles simulated, the accuracy of the time and intensity predictions over the period 1933–2018 are still comparable within uncertainties between the two works. The incorporation of the comet's $Af\rho$ evolution into the model allowed (Egal et al., 2018) to obtain correct time and ZHR estimates for historic Draconid outbursts and to perform a high-fidelity prediction of the 2018 outburst (cf. Section 8). In this work, the incorporation within the weighting solution of new measurements of the comet's activity (including post-perihelion observations) allowed an increase in the accuracy of our modeling. At the same time, the calibration process maintained consistency with our previous work despite significant variations of our ZHR profile computation.

10.2.1. Potential 2019 outburst

As described in Section 9, a prediction for the 2019 Draconids was particularly difficult to establish and our results diverge from other studies. The low resolution of the simulated activity profile hampers a reliable peak time estimate, while the maximum intensity prediction is complicated by a few unphysically heavily-weighted 1966 particles that we chose to remove. Nevertheless, we predict a radio outburst on October 8 around 12h UT; most other authors expect a lower maximum activity later the same day. Radar observations of the 2019 Draconids will therefore be a good opportunity to both test and improve our model. Precise measurements would help to determine the veracity of our choice to limit the contribution of the 1966 stream, as well as the ephemeris computation implemented in our model.

The 2019 Draconid return will also offer the opportunity to study two of the most problematic trails in the Draconid complex. The 1959 and 1966 streams, both of which cross the Earth's trajectory in 2019, previously encountered the planet in 1999 and caused a strong radio outburst that was unnoticed until this work. They also intercepted the Earth in 2012, producing a radio storm that was unpredicted by every shower modeler. The fact that 21P suffered an orbital discontinuity precisely during the period 1959–1965 might also point to the activation of local source regions over the comet's surface (Sekanina, 1993) and a potential for much higher activity than that considered in this model. Special attention should therefore be paid to observations of the coming shower on October 8, 2019.

11. Conclusion

In this work, we performed numerical simulations of comet 21P/Giacobini-Zinner and the Draconid meteoroid stream complex following the methodology of Vaubaillon et al. (2005). We generated a total of about 22 million dust particles, ejected by the comet since 1850. Particles were integrated until the year 2030, and candidates approaching the Earth were carefully selected and analyzed in order to identify past and future Draconid outbursts.

To our knowledge, this study is the first to produce ZHR profiles for each simulated Draconid shower and quantitatively estimate the peak time and intensity of all the reported historic outbursts. Our model

provides a timing accuracy of order half an hour for the peak times and a ZHR estimate correct to within a factor of 2 (visual showers) or 3 (radio outbursts). These successful post-predictions are the result of an updated weighting scheme of the simulated meteoroids, allowing us to better assess the contribution of individual particles to the shower. The initial algorithm of Vaubaillon et al. (2005) has been updated and modified to take into account the evolution of the parent comet dust production along its orbit, adjusted using recent measurements of 21P performed by the NASA Meteoroid Environment Office between May and December 2018. Thanks to this updated solution, we were able to uncover the existence of a previously unreported strong radio outburst in 1999 that we confirmed by archival radar measurements at the predicted date and time. A first set of simulations issued from this model also led to one of the best published predictions of the recent 2018 outburst (Egal et al., 2018).

In the next decade, we can expect up to three Draconid outbursts caused by radar-sized meteoroids, respectively in 2019, 2025 and potentially 2029. Observations of the 2019 outburst, which we find is among the most challenging of all returns to characterize from our simulations, should particularly help in improving our stream modeling for the Draconid returns of the 2020s.

From our model predictions, we expect a strong radio outburst on October 8, 2025 and a somewhat weaker shower in 2019. We encourage observers to be particularly vigilant in recording the Draconid shower in these years.

Acknowledgements

Appendix A. Ejection velocity

In this work, we compared the performance of different ejection velocity models, using the parameters of Table 1. Four ejection models were specifically investigated: the original Whipple formula (Whipple, 1951), the Jones model (Jones, 1995, $r_h^{-1.038}$), the Jones model as modified by Brown and Jones (1998), $r_h^{-0.5}$, and the Crifo and Rodionov (1997) model. The analytical expression of each ejection velocity implemented is given in Eq. (A.1), and the corresponding distributions are presented in Fig. A.7.

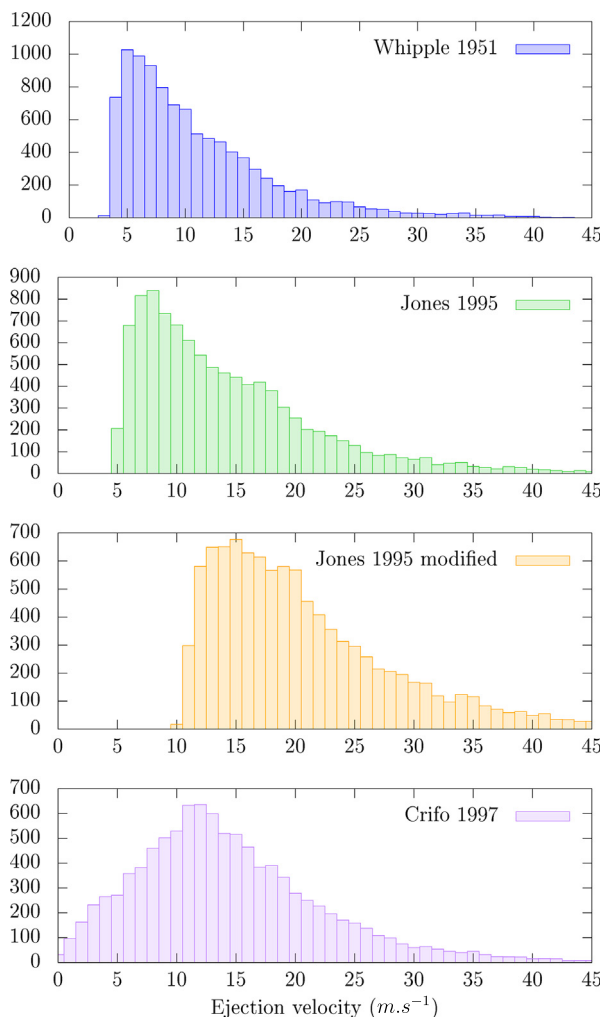**Fig. A.7.** Ejection velocity distributions generated using the parameters of Table 1 for different models.

Whipple 1951: $V_{ej} = \sqrt{r_c \left(\dfrac{43}{a\rho r_h^{2.25}} - \dfrac{8\pi \mathscr{G} \rho_c r_c}{3} \right)}$

Jones 1995: $V_{ej} = 10.2 r_h^{-1.038} \rho^{-1/3} \sqrt{r_c}\, m^{-1/6}$

Modified: $V_{ej} = 10.2 r_h^{-0.5} \rho^{-1/3} \sqrt{r_c}\, m^{-1/6}$

Crifo 1997: $V_{ej} = \dfrac{W}{1.2 + 0.72 \sqrt{\dfrac{a}{a \star}}}$ (cf. Eq.)

(A.1)

Recent measurements performed by the Rosetta spacecraft around comet 67P/Churyumov-Gerasimenko suggest that the real ejection velocities of dust particles are much lower than the speeds usually considered by these models. As an example, most of the compact grains with masses of $[10^{-10}, 10^{-7}]$ kg detected by the Grain Impact Analyser and Dust Accumulator (GIADA) instrument displayed velocities ranging from 0.3 to 12.2 m/ s (Della Corte et al., 2015). When looking at the distribution profiles drawn in Fig. A.7 we see that among the four formulas considered, the Crifo and Rodionov (1997) model is the most efficient in ejecting particles with low speeds ($\in]0, 5]$ m/s). As in Vaubaillon et al. (2005), we therefore decided to utilize this ejection model for our simulations.

Appendix B. 21P's $Af\rho$ evolution

In our weighting model (cf. C), we assume that the $Af\rho$ parameter defined by A'Hearn et al. (1984) directly reflects the number of dust particles ejected by comet 21P. The number of real meteoroids associated with each simulated particle therefore depends on the evolution of $Af\rho$ with the comet heliocentric distance. Quantities implied in this parameter are (A'Hearn et al., 1984):

1. A: the albedo $A(\Phi) = 4\pi A_B j(\Phi)$, which depends on the Bond albedo A_B and the normalized phase function $j(\Phi)$ at angle Φ
2. f: the filling factor of the dust grains within the field of view, usually computed as the sum of the particles geometric cross sections divided by the area of the field of view
3. ρ: the aperture radius used for the observation. This factor was added to make the $Af\rho$ parameter independent of the field of view observed. This assumption is asserted in the case of a simple radial-outflow cometary model with a brightness profile evolving as $1/\rho$.

While the brightness profile of comet 21P/Giacobini-Zinner may obey a ρ^{-1} dependence within a limited central region, the profile will eventually steepen for larger aperture radii (Jewitt and Meech, 1987). For this reason and because of the suspected variability of 21P's coma brightness on a daily time scale, one needs to be very cautious in comparing $Af\rho$ measurements of the comet performed at different epochs using different instruments and reduction techniques. Despite numerous observations of 21P performed since 1985 (e.g. Blaauw et al., 2014; Lara et al., 2003; Pittichová et al., 2008; Schleicher et al., 1987; Singh et al., 1997), no general agreement in the $Af\rho$ estimates of the comet was reached for both the pre- and the post-perihelion branch of its orbit. To addressthis issue, an unprecedented observation campaign targeting 21P has been undertaken by the NASA Meteoroid Environment Office in May 2018, starting five months before the perihelion approach and continuing until 2019.

Telescopic observations of Comet 21P were taken on 65 nights spanning from 2018-05-05 through 2018-12-18 using publicly accessible tele- scopes owned and operated by iTelescope.[4] In particular, we utilized telescopes T11 in Mayhill New Mexico, T7 in Nerpio Spain, and T30/T31 at Siding Spring Observatory in Australia. These observations imaged the comet during its ingress phase at heliocentric distances ranging from 1.93 AU through perihelion (1.01 AU) and during its egress phase back out to 1.66 AU. Telescope T7 in Spain has a primary mirror diameter of 0.41 m, while the other three telescopes all have primary mirrors 0.50 m in diameter. Ten images of the comet were taken each night using the Johnson-Cousins R_C band filter, with exposure times ranging from 15 s to 1 min based on the non-sidereal motion of the comet. Determinations of $Af\rho$ for each set of images were performed in a manner nearly identical to the one described in Blaauw et al. (2014) and Hosek Matthew et al. (2013). Just like in these works, the $Af\rho$ measurements are performed within a $10'' \times 10''$ square aperture centered on the brightest pixel associated with the comet emission. Further details on the observation campaign and the derived $Af\rho$ values are discussed in Ehlert et al. (in preparation).

A first analysis showed a noticeable asymmetry between the ascending activity branch (pre-perihelion measurements) and the descending branch (post-perihelion). When fitting each branch with a logarithmic function of the form $Af\rho(r_h) = K_1 + K_2 r_h^{\gamma} mma$, best fits were obtained for a loga- rithmic slope $\gamma = -5.5$ for the ascending branch and $\gamma = -15.5$ for the descending branch. However, no accurate fit of both branches was obtained when forcing the extrapolated maximal $Af\rho$ value to be identical for each fit. Because the weighting solution requires an analytical expression of $Af\rho = f(r_h)$ over all the comet orbit, we decided to adjust preliminary $Af\rho$ measurements with a standard double-exponential shape function of the form:

$$\begin{cases} Af\rho(X) = K_1 + Af\rho(X_{\max}) * 10^{-\gamma|X - X_{\max}|} \\ \gamma = \gamma_1 \text{ if } X \geq X_{\max} \text{ and } \gamma = \gamma_2 \text{ if } X \leq X_{\max} \\ X = (r_h - q) \dfrac{t(q) - t}{|t(q) - t|} \end{cases}$$

(B.1)

The best agreement with 21P's observations was reached for $K_1 \sim 100$, $Af\rho(X_{\max}) \sim 1650$, $\gamma_1 = 2.0$, $\gamma_2 = 7.0$ and $X_{\max} = 0.04$, and illustrated by Fig. B.8. Fit attempts using Gaussian, Lorentzian or Moffat functions were not more successful than the double-exponential shape model in re- producing the observations of the comet.

As already noticed by several authors (e.g. Blaauw et al., 2014; Lara et al., 2003), preliminary observations performed in 2018 indicate a cometary activity not peaking exactly at the perihelion ($X_{\max} \neq 0$). It is assumed that the gas and dust productions peak before the perihelion since ~1960, when the comet suffered dramatic changes in its non-gravitational coefficients (Blaauw et al., 2014; Sekanina, 1985). In 2018, the maximum dust production of the comet is observed a few days before the perihelion passage. This time shift varied for each apparition of the comet, reaching a value of about one month in 1985 (McFadden et al., 1987; Schleicher et al., 1987). Because of the lack of information regarding the asymmetric

---

[4] https://www.itelescope.net/
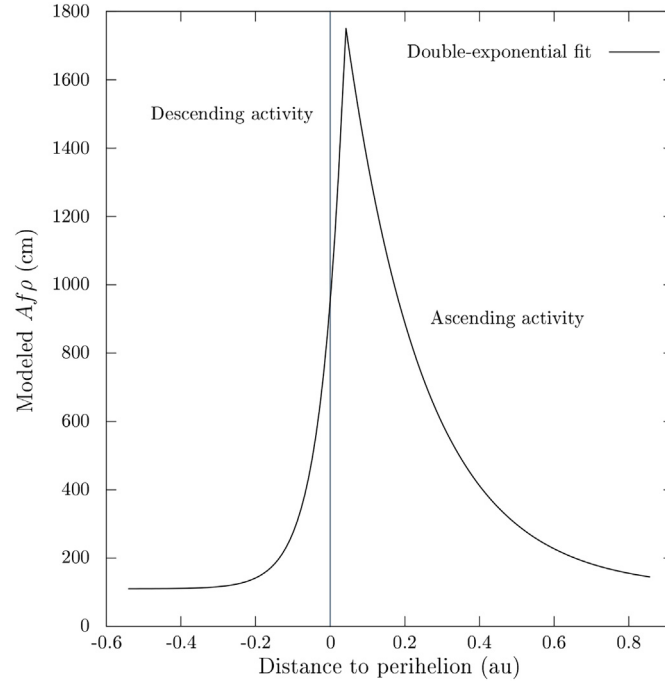
Fig. B.8. Modelled *Af*p dependence with the distance to perihelion for 21P's 2018 apparition. The abscissa represents the heliocentric distance to perihelion, arbitrarily positive for pre-perihelion measurements and negative for post-perihelion dust production ($X = (r_h - q)\frac{t(q)-t}{|t(q)-t|}$, with $t(q)$ the time at perihelion).

outgassing of the comet at each apparition, we however will consider that the maximum outgassing of the comet and its perihelion passage coincides for each apparition considered in our simulations ($X_{max} = 0$).

For the same reason, we are also forced to assume that the cometary dust emission with the heliocentric distance is similar for all orbits considered. $Af\rho(r_h)$ estimates for ancient locations of the comet therefore only rely on its orbital characteristics (e.g. perihelion distance and semi-major axis). Even if these assumptions are likely erroneous given the variability of 21P, they provide a first approximation of the dust emission evolution for each apparition of the comet.

Appendix C. Weighting scheme

This appendix summarizes the steps we take to determine the total number of meteoroids ejected by the comet at a given location. For more information, the reader is referred to Vaubaillon et al. (2005).

C.1. Gas production rate

We assume that the comet's outgassing is dominated by the sublimation of water ice. The global gas production rate $Q_{H_2O}(r_h)$ is a function of the heliocentric distance r_h. In this model, the water molecules and dust particles are ejected from the sunlit hemisphere of a spherical and homogeneous nucleus. The intensity of the gas production depends on the cosine of the angle θ between the ejection direction and the subsolar point. The effective sublimation rate for a unit area at the surface of the comet is then expressed as

$$Z_{H_2O}(r_h, \theta) = Q_{H_2O}(r_h)\frac{cos\ \theta}{\pi R_c^2}$$

(C.1)

where R_c is the radius (in km) of the comet's nucleus.

C.2. Dust production rate

At a heliocentric distance r_h, the local dust sublimation rate Z_g (in $m^{-2}\ s^{-1}$) is related to the local ice sublimation rate by a variable dust-to-gas ratio $K(r_h)$:

$$Z_g(r_h, \theta) = K(r_h)Z_{H_2O}(r_h, \theta)$$

(C.2)

In contrast with Vaubaillon et al. (2005), we do not assume that the function K is independent of heliocentric distance. In order to correlate the local dust sublimation rate with observable measurements of the particles released by the comet, it is necessary to adopt a definite size distribution of the dust particles at ejection. Following Vaubaillon et al. (2005), we assume that the size distribution h of the particles follows a power law of index u such that

$$h(a) = \frac{N}{a^u}$$

(C.3)

where a is the radius of the particles in m and N is a normalization constant solution of the equation $\int_{a_1}^{a_2} h(a)da = 1$. The differential local dust sublimation rate for a particle of size a becomes

$$Z_g(r_h, \theta, a) = K(r_h) Q_{H_2O}(r_h) \frac{\cos \theta}{\pi R_c^2} \frac{N}{a^u}$$

(C.4)

The parameter $K(r_h)$ is determined from the $Af\rho$ measurement at the heliocentric distance r_h. Using Eq. (C.4), the density n_g of particles of radius $a \in [a_1, a_2]$ around the nucleus is given by

$$n_g(a, \theta, d, r_h) = \frac{Z_g(r_h, \theta, a)}{v_g(r_h, \theta, a)} \left(\frac{R_c}{d}\right)^2$$

(C.5)

where d is the distance to the nucleus (in km) and v_g is the dust terminal velocity in (m s^{-1}). The radii a_1 & a_2 represent respectively the minimal and maximal radius of a particle that can be ejected by the comet. The dust terminal velocity depends on the ejection model and the size and density of the particles considered. For the Crifo and Rodionov (1997) ejection model, the terminal velocity of a particle with radius a, ejected at r_h for an angle θ between the ejection direction and the subsolar point is

$$v_g(a, \theta, r_h) = W\phi(\theta, a) = \frac{W}{\alpha + \beta \sqrt{\frac{a}{\cos(\theta)}}}$$

$$\text{where } W = \sqrt{\frac{\gamma_{H_2O} + 1}{\gamma_{H_2O} - 1} \frac{\gamma_{H_2O} k_B T}{m}}$$

(C.6)

and

- $\gamma_{H_2O} = \frac{4}{3}$ is the ratio of the specific water heats,
- k_B is the Boltzmann constant,
- T is the gas temperature,
- m is the mass of gas molecules (18 amu),

$\alpha = 1.2$,

- $\beta = 0.72/\sqrt{a_\star^0}$, where $a_\star^0$ is the critical radius of the particle below which the gas-particle interaction efficiency starts to decrease. For $a < < a_\star^0$, $v_g(a, \theta, r_h) \simeq W$ (Crifo and Rodionov, 1997).

The spatial density n_g can be correlated after integration to the filling factor parameter of the $Af\rho$ measurement. Considering the Crifo and Rodionov (1997) ejection model, the relation between the local dust sublimation rate and the $Af\rho$ parameter allows us to derive the expression of $K(r_h)$:

$$K(r_h) = \frac{J Af\rho(r_h)}{2N Q_{H_2O}(r_h) A(\Phi)}$$

(C.7)

where $J = \frac{W}{[\alpha A_3(a_1; a_2) + \beta I A_{3.5}(a_1; a_2)]}$, $I = \frac{1}{2} B\left(\frac{3}{4}; \frac{1}{2}\right)$ with B the Beta function (Abramowitz and Stegun, 1972) and A_x the solution of the integral $\int_{a_1}^{a_2} \frac{da}{a^{u-x+1}}$ (Vaubaillon et al., 2005). The parameter $A(\Phi)$ represents the albedo of the nucleus at the phase angle Φ.

The differential local dust sublimation rate is finally

$$Z_g(r_h, \theta, a) = \frac{J Af\rho(r_h)}{2A(\Phi)} \frac{\cos \theta}{\pi R_c^2} \frac{1}{a^u}$$

(C.8)

The total number of meteoroids ejected in the size range $[a_1', a_2']$, in a differential region around r_h at the ejection angles (θ, ϕ) during a period Δt is

$$N_g = N_g(r_h, a_1', a_2')$$
$$= R_c^2 \Delta t \int_{\theta - \frac{\Delta \theta}{2}}^{\theta + \frac{\Delta \theta}{2}} \int_{\phi - \frac{\Delta \phi}{2}}^{\phi + \frac{\Delta \phi}{2}} \int_{r_h - \frac{\Delta r_h}{2}}^{r_h + \frac{\Delta r_h}{2}}$$
$$\int_{a_1'}^{a_2'} Z_g(r_h, \theta, a') \sin \theta \, da' dr_h d\phi d\theta$$

(C.9)

i.e.

$$N_g = R_c^2 \Delta t \int_\theta \int_\phi \int_{r_h} \int_{a'} \frac{J Af\rho(r_h)}{2A(\Phi)} \frac{\cos \theta}{\pi R_c^2}$$
$$\times \frac{1}{a'^u} \sin \theta \, da' dr_h d_\phi d\theta$$
$$= \frac{\Delta t J}{2\pi A(\Phi)} \int_\theta \sin \theta \cos \theta \, d\theta \int_\phi d\phi \int_{r_h} Af\rho(r_h) dr_h \int_{a'} \frac{1}{a'^u} da'$$

(C.10)

For $\theta \in [0, \frac{\pi}{2}]$ and $\phi \in [0, 2\pi]$ we obtain

$$N_g = \frac{J \Delta t}{2A(\Phi)} A_1(a_1', a_2') \int_{r_h} Af\rho(r_h) dr_h$$

(C.11)

If we assume that $Af\rho(r_h) = K_1 + Af\rho_{max} \cdot 10^{-\gamma(r_h - q)}$, with q the perihelion distance and $\gamma = \gamma_1$ pre-perihelion and $\gamma = \gamma_2$ post-perihelion (cf. B, with $Afrho_{max} = Af\rho(X_{max})$ and $X_{max} = 0$), then.

$$I_{Af\rho} = \int_{r_h - \frac{\Delta r_h}{2}}^{r_h + \frac{\Delta r_h}{2}} Af\rho(r_h) dr_h = K_1 \Delta r_h - \frac{Af\rho_{max}}{\gamma \ln(10)} [10^{-\gamma(r_h - q)}]_{r_h - \frac{\Delta r_h}{2}}^{r_h + \frac{\Delta r_h}{2}}$$

(C.12)

and Eq. (C.11) leads to:

$$N_g = \frac{J\Delta t}{2A(\Phi)} A_1(a_1', a_2') \cdot \left(K_1 \Delta r_h \frac{1}{2} - \frac{Af\rho_{max}}{\gamma \ln(10)} [10^{-\gamma(r_h - q)}]_{r_h - \frac{\Delta r_h}{2}}^{r_h + \frac{\Delta r_h}{2}} \right)$$

(C.13)

For a given apparition of the comet with a perihelion distance q, the number of particles ejected in all directions in the size bin $[a_1', a_2']$ during Δt around r_h is finally:

$$\begin{cases} N_g = K_2 \frac{J\Delta t}{2A(\Phi)} A_1(a_1', a_2') \cdot \left(K_1 \Delta r_h \frac{1}{2} \right. \\ - \frac{Af\rho_{max}}{\gamma \ln(10)} \left[10^{-\gamma\left(r_h + \frac{\Delta r_h}{2} - q\right)} - 10^{-\gamma\left(r_h - \frac{\Delta r_h}{2} - q\right)} \right] \right) \\ \gamma = \gamma_1 \text{ pre} - \text{perihelion and } \gamma = \gamma_2 \text{ post} - \text{perihelion} \end{cases}$$

(C.14)

The optional K_2 proportionality coefficient, constant over all the ejection circumstances, allow to account for systematic biases in the estimate of the intensity of the cometary activity. This parameter, as well as the size distribution index u can be calibrated on previous meteor observations.

References

Abramowitz, M., Stegun, I.A., 1972. Handbook of Mathematical Functions.

A'Hearn, M.F., Schleicher, D.G., Feldman, P.D., Millis, R.L., Thompson, D.T., 1984. Comet Bowell 1980b. Astron. J. 89.

Arlt, R., 1998. Summary of 1998 Draconid outburst observations. WGN, Journal of the International Meteor Organization 26, 256–259.

Blaauw, R.C., Suggs, R.M., Cooke, W.J., 2014. Dust production of comet 21P/Giacobini-Zinner using broadband photometry. Meteorit. Planet. Sci. 49, 1–10.

Borovička, J., Spurný, P., Koten, P., 2007. Atmospheric deceleration and light curves of Draconid meteors and implications for the structure of cometary dust. Astron. Astrophys. 473, 661–672. https://doi.org/10.1051/0004-6361:20078131.

Brown, P., Jones, J., 1998. Simulation of the formation and evolution of the Perseid meteoroid stream. Icarus 133, 36–68. https://doi.org/10.1006/icar.1998.5920.

Brown, P., Campbell, M.D., Ellis, K.J., Hawkes, R.L., Jones, J., Gural, P., Babcock, D., Barnbaum, C., Bartlett, R.K., Bedard, M., Bedient, J., Beech, M., Brosch, N., Clifton, S., Connors, M., Cooke, B., Goetz, P., Gaines, J.K., Gramer, L., Gray, J., Hildebrand, A.R., Jewell, D., Jones, A., Leake, M., LeBlanc, A.G., Looper, J.K., McIntosh, B.A., Montague, T., Morrow, M.J., Murray, I.S., Nikolova, S., Robichaud, J., Spondor, R., Talarico, J., Theijsmeijer, C., Tilton, B., Treu, M., Vachon, C., Webster, A.R., Weryk, R., Worden, S.P., 2000. Global ground-based electro-optical and radar observations of the 1999 Leonid shower: first results. Earth Moon and Planets 82, 167–190.

Campbell-Brown, M., Vaubaillon, J., Brown, P., Weryk, R.J., Arlt, R., 2006. The 2005 Draconid outburst. Astron. Astrophys. 451, 339–344. https://doi.org/10.1051/0004-6361/20054588.

Chebotarev, R.P., Simek, M., 1987. The structure of the Giacobinid 1985 meteor shower from radar observations in Dushanbe and Ondrejov. Bulletin of the Astronomical Institutes of Czechoslovakia 38, 362–367.

Churyumov, K.I., Rosenbush, V.K., 1991. Peculiarities of gas and dust production rates in comets P/Halley (1986III), P/Giacobini-Zinner (1985 XIII), P/Hartley-Good (1985 XVII) and P/Thiele (1985XIX). Astron. Nachr 312, 385–391.

Cook, A.F., 1973. A working list of meteor streams. NASA Special Publication 319, 183.

Crifo, J.F., Rodionov, A.V., 1997. The dependence of the circumnuclear coma structure on the properties of the nucleus. Icarus 127, 319–353. https://doi.org/10.1006/icar.1997.5690.

Davies, J.G., Lovell, A.C.B., 1955. The Giacobinid meteor stream. Monthly Notices of the RAS 115, 23. https://doi.org/10.1093/mnras/115.1.23.

Della Corte, V., Rotundi, A., Fulle, M., Gruen, E., Weissman, P., Sordini, R., Ferrari, M., Ivanovski, S., Lucarelli, F., Accolla, M., Zakharov, V., Mazzotta Epifani, E., Lopez-Moreno, J.J., Rodriguez, J., Colangeli, L., Palumbo, P., Bussoletti, E., Crifo, J.F., Esposito, F., Green, S.F., Lamy, P.L., McDonnell, J.A.M., Mennella, V., Molina, A., Morales, R., Moreno, F., Ortiz, J.L., Palomba, E., Perrin, J.M., Rietmeijer, F.J.M., Rodrigo, R., Zarnecki, J.C., Cosi, M., Giovane, F., Gustafson, B., Herranz, M.L., Jeronimo, J.M., Leese, M.R., Lopez-Jimenez, A.C., Altobelli, N., 2015. Giada: shining a light on the monitoring of the comet dust production from the nucleus of 67p/Churyumov-Gerasimenko. A&A 583, A13. https://doi.org/10.1051/0004-6361/201526208 https://doi.org/10.1051/0004-6361/201526208.

Denning, W.F., 1927. La Nouvelle Chute Meteorique Cometaire. L'Astronomie 41, 374–376.

Egal, A., Wiegert, P., Brown, P.G., Moser, D.E., Moorhead, A.V., Cooke, W.J., 2018. The Draconid Meteoroid Stream 2018: Prospects for Satellite Impact Detection. vol. 866. pp. L8. https://doi.org/10.3847/2041-8213/aae2ba.. arXiv:1809.07393.

Everhart, E., 1985. An efficient integrator that uses Gauss-Radau spacings. International Astronomical Union Colloquium 83, 185â€"202.

Fisher, W.J., 1934. The history of the Giacobinid meteors. Harvard College Observatory Bulletin 894, 15–16.

Fujiwara, Y., Kero, J., Abo, M., Szasz, C., Nakamura, T., 2016. MU radar head echo observations of the 2012 October Draconid outburst. Mon. Not. R. Astron. Soc. 455,

3273–3280. https://doi.org/10.1093/mnras/stv2492.

Fulle, M., Marzari, F., Della Corte, V., Fornasier, S., Sierks, H., Rotundi, A., Barbieri, C., Lamy, P.L., Rodrigo, R., Koschny, D., Rickman, H., Keller, H.U., López-Moreno, J.J., Accolla, M., Agarwal, J., A'Hearn, M.F., Altobelli, N., Barucci, M.A., Bertaux, J.L., Bertini, I., Bodewits, D., Bussoletti, E., Colangeli, L., Cosi, M., Cremonese, G., Crifo, J.F., Da Deppo, V., Davidsson, B., Debei, S., De Cecco, M., Esposito, F., Ferrari, M., Giovane, F., Gustafson, B., Green, S.F., Groussin, O., Grün, E., Gutierrez, P., Güttler, C., Herranz, M.L., Hviid, S.F., Ip, W., Ivanovski, S.L., Jerónimo, J.M., Jorda, L., Knollenberg, J., Kramm, R., Kührt, E., Küppers, M., Lara, L., Lazzarin, M., Leese, M.R., López-Jiménez, A.C., Lucarelli, F., Mazzotta Epifani, E., McDonnell, J.A.M., Mennella, V., Molina, A., Morales, R., Moreno, F., Mottola, S., Naletto, G., Oklay, N., Ortiz, J.L., Palomba, E., Palumbo, P., Perrin, J.M., Rietmeijer, F.J.M., Rodríguez, J., Sordini, R., Thomas, N., Tubiana, C., Vincent, J.B., Weissman, P., Wenzel, K.P., Zakharov, V., Zarnecki, J.C., 2016. Evolution of the dust size distribution of comet 67P/Churyumov-Gerasimenko from 2.2 au to perihelion. Astrophys. J. 821, 19. https://doi.org/10.3847/0004-637X/821/1/19.

Green, S.F., McDonnell, J.A.M., McBride, N., Colwell, M.T.S.H., Tuzzolino, A.J., Economou, T.E., Tsou, P., Clark, B.C., Brownlee, D.E., 2004. The dust mass distribution of comet 81p/wild 2. Journal of Geophysical Research: Planets 109. https://doi.org/10.1029/2004JE002318.

Hanner, M.S., Veeder, G.J., Tokunaga, A.T., 1992. The dust coma of comet P/Giacobini-Zinner in the infrared. Astron. J. 104, 386–393.

Hosek Matthew, W.J., Blaauw, R.C., Cooke, W.J., Suggs, R.M., 2013. Outburst Dust Production of Comet 29P/Schwassmann-Wachmann 1. vol. 145. pp. 122. https://doi.org/10.1088/0004-6256/145/5/122.

Hughes, D.W., Thompson, D.A., 1973. The Giacobinid (Draconid) meteor shower, 1972. Monthly Notices of the RAS 163 (3P). https://doi.org/10.1093/mnras/163.1.3P.

Hutcherson, W.R., 1946. Spectacular shower of meteors observed in Berea, Kentucky. Popular Astronomy 54, 484.

Jenniskens, P., 1995. Meteor stream activity. 2: meteor outbursts. Astron. Astrophys. 295, 206–235.

Jenniskens, P., 2006. Meteor Showers and their Parent Comets.

Jewitt, D.C., Meech, K.J., 1987. Surface Brightness Profiles of 10 Comets. vol. 317. pp. 992–1001. https://doi.org/10.1086/165347.

Jodrell Bank, 1953. Report on Jodrell Bank to the Royal Astronomical Society Council for 1953. In: Proceedings of Observatories - Jodrell Bank Reprint no 97.

Jones, J., 1995. The ejection of meteoroids from comets. Monthly Notices of the RAS 275, 773–780. https://doi.org/10.1093/mnras/275.3.773.

Kac, J., 2015. Draconid 2011 outburst observations from Slovenia. WGN, Journal of the International Meteor Organization 43, 75–80.

Kastinen, D., Kero, J., 2017. A Monte Carlo-type simulation toolbox for solar system small body dynamics: application to the October Draconids. Planetary Space Science 143, 53–66. https://doi.org/10.1016/j.pss.2017.03.007.

Kero, J., Fujiwara, Y., Abo, M., Szasz, C., Nakamura, T., 2012. MU radar head echo observations of the 2011 October Draconids. Monthly Notices of the RAS 424, 1799–1806. https://doi.org/10.1111/j.1365-2966.2012.21255.x.

Koschack, R., Rendtel, J., 1990. Determination of spatial number density and mass index from visual meteor observations (I). WGN, Journal of the International Meteor Organization 18, 44–58.

Koseki, M., 1990. Observations of the 1985 Giacobinids in Japan. Icarus 88, 122–128. https://doi.org/10.1016/0019-1035(90)90181-8.

Koseki, M., Teranishi, K., Shiba, J., Sekiguchi, Y., 1998. Giacobinids returned in the Japanese sky: video and photographic observations. WGN. Journal of the International Meteor Organization 26, 260–262.

Koten, P., Borovička, J., Spurný, P., Štork, R., 2007. Optical observations of enhanced activity of the 2005 Draconid meteor shower. Astron. Astrophys. 466, 729–735. https://doi.org/10.1051/0004-6361:20066838.

Koten, P., Vaubaillon, J., Tóth, J., Margonis, A., Ďuriš, F., 2014. Three peaks of 2011 Draconid activity including that connected with pre-1900 material. Earth Moon and

Planets 112, 15–31. https://doi.org/10.1007/s11038-014-9435-9.

Kresák, L., 1993. Meteor storms (invited). In: Stohl, J., Williams, I.P. (Eds.), Meteoroids and their Parent Bodies, pp. 147.

Kresak, L., Slancikova, J., 1975. On the structure of the Giacobinid meteor shower. Bulletin of the Astronomical Institutes of Czechoslovakia 26, 327–342.

Królikowska, M., Sitarski, G., Szutowicz, S., 2001. Forced Precession Models for Six Erratic Comets M. A&Ahttps://doi.org/10.1051/0004-6361. (arXiv:arXiv:0709.4560v1).

Lamy, P.L., Toth, I., Fernandez, Y.R., Weaver, H.A., 2004. The Sizes, Shapes, Albedos, and Colors of Cometary Nuclei. pp. 223–264.

Landaberry, S.J.C., Singh, P.D., Pacheco, J.A.d.F., 1991. Ground-based observations of comets Giacobini-Zinner (1984e) and Hartley-good (1985I). Astron. Astrophys. 246, 597–602 DOI:1991A&A...246..597L.

Langbroek, M., 1999. The 1999 Draconids from the Netherlands and the Draconids of 1953. WGN. Journal of the International Meteor Organization 27, 335–338.

Lara, L.M., Licandro, J., Oscoz, A., Motta, V., 2003. Behaviour of Comet 21P/Giacobini-Zinner during the 1998 Perihelion. A&A.

Leibowitz, E.M., Brosch, N., 1986. Periodic photometric variations in the near-nucleus zone of P/Giacobini-Zinner. Icarus 68, 430–441. https://doi.org/10.1016/0019-1035(86)90049-7.

Lindblad, B.A., 1987. The 1985 return of the Giacobinid meteor stream. Astron. Astrophys. 187, 928.

Lovell, A.C.B., Banwell, C.J., Clegg, J.A., 1947. Radio echo observations of the Giacobinids meteors, 1946. Monthly Notices of the RAS 107, 164. https://doi.org/10.1093/mnras/107.2.164.

Marsden, B.G., 1972. IAU Circular No 2451.

Marsden, B.G., Sekanina, Z., 1971. Comets and nongravitational forces. IV. Astron. J. 76, 1135. https://doi.org/10.1086/111232.

Maslov, M., 2011. Future Draconid outbursts (2011 − 2100). WGN, Journal of the International Meteor Organization 39, 64–67.

Mason, J.W., 1986. Giacobinid meteor stream activity in October 1985. In: Battrick, B., Rolfe, E.J., Reinhard, R. (Eds.), ESLAB Symposium on the Exploration of Halley's Comet.

McBeath, A., 2012. SPA meteor section results: radio Draconids 2011. WGN, Journal of the International Meteor Organization 40, 126–128.

McDonnell, J.A.M., Evans, G.C., Evans, S.T., Alexander, W.M., Burton, W.M., Firth, J.G., Bussoletti, E., Grard, R.J.L., Hanner, M.S., Sekanina, Z., 1987. The Dust Distribution within the Inner Coma of Comet P/Halley 1982i — Encounter by Giotto's Impact Detectors. vol. 187. pp. 719–741.

McFadden, L.A., A'Hearn, M.F., Feldman, P.D., Bohnhardt, H., Rahe, J., Festou, M.C., 1987. Ultraviolet spectrophotometry of comet Giacobini-Zinner during the ICE encounter. Icarus 337.

McIntosh, B.A., 1972. Giacobinid meteor shower: prospect for 1972. Journal of the RAS of Canada 66, 149.

Millman, P.M., 1973. Meteor news: airborne observations of the 1972 Giacobinids. J. R. Astron. Soc. Can. 67, 35.

Molau, S., Barentsen, G., 2014. Real-time flux density measurements of the 2011 Draconid meteor outburst. Earth Moon and Planets 112, 1–5. https://doi.org/10.1007/s11038-013-9425-3. arXiv:1312.3605.

Moser, D., 2018. MSFC meteoroid stream model results, 2019. Technical report. JPID-FY18–02018.

Moser, D.E., Cooke, W.J., 2004. Msfc stream model preliminary results: modeling recent Leonid and Perseid encounters. Earth Moon Planet. 95, 141–153. URL: https://doi.org/https://doi.org/10.1007/s11038-005-3185-7, (doi:10.1007/s11038-005-3185-7).

Moser, D.E., Cooke, W.J., 2008. Updates to the MSFC meteoroid stream model. Earth Moon and Planets 102, 285–291. https://doi.org/10.1007/s11038-007-9159-1.

Newburn, R.L., Spinrad, H., 1985. Spectrophotometry of seventeen comets. II. The continuum. Astron. J. 90, 2591–2608.

Newburn, R.L., Spinrad, H., 1989. Spectrophotometry of 25 comets — post-Halley updates for 17 comets plus new observations for eight additional comets. 97, 552–569. https://doi.org/10.1086/115005.

Olivier, C.P., 1946. Meteor notes from the American Meteor Society. Popular Astronomy 54, 475.

Pittichová, J., Woodward, C.E., Kelley, M.S., Reach, W.T., 2008. Ground-based optical and Spitzer infrared imaging observations of comet 21P/Giacobini-Zinner. Astron. J. 136, 1127–1136. https://doi.org/10.1088/0004-6256/136/3/1127. arXiv:0806.3582.

Plavec, M., 1957. Vznik a Rana Vyvojova Stadia Meteorickyck Roju. On the Origin and Early Stages of the Meteor Streams. Publications of the Astronomical Institute of the Czechoslovak Academy of Sciences 30.

Pokorný, P., Brown, P.G., 2016. A Reproducible Method to Determine the Meteoroid Mass Index. vol. 592. pp. A150. https://doi.org/10.1051/0004-6361/201628134.. arXiv:1605.04437.

Reznikov, E.A., 1993. The Giacobini-Zinner comet and Giacobinid meteor stream. Trudy Kazan. Gor. Astron. Obs. 53, 80–101.

Sato, M., 2003. An investigation into the 1998 and 1999 Giacobinids by meteoroid trajectory modeling. WGN. Journal of the International Meteor Organization 31, 59–63.

Schleicher, D.G., Millis, R.L., Birch, P.V., 1987. Photometric Observations of Comet P/Giacobini-Zinner. A&A.

Sekanina, Z., 1985. Precession model for the nucleus of periodic comet Giacobini/Zinner. Astron. J. 90.

Sekanina, Z., 1993. Effects of discrete-source outgassing on motions of periodic comets and discontinuous orbital anomalies. Astron. J. 105, 702–735. https://doi.org/10.1086/116468.

Sidorov, V.V., Stepanov, A.M., Sulejmanov, N.I., 1994. Observations of the Draconid meteor stream in Kazan in 1985. Sol. Syst. Res. 28, 190–193.

Sigismondi, C., 2011. Airborne observation of 2011 Draconids meteor outburst: the Italian mission. ArXiv e-prints arXiv:1112.4873.

Simek, M., 1994. Fine structure of the 1985 Giacobinids. Astron. Astrophys. 284, 276–280.

Šimek, M., Pecina, P., 1999. The Giacobinid meteor stream observed by radar in 1998. Astron. Astrophys. 343, L94–L96.

Singh, P.D., Huebner, W.F., Costa, R.D.D., Landaberry, S.J.C., Pacheco, J.A.d.F., 1997. Gas and dust release rates and color of dust in comets P/Halley (1986 III), P/G iacobini-Zinner (1985 XIII), and P/Hartley-Good (1985 XVII). Planet. Space Sci. 45.

Southworth, R.B., Hawkins, G.S., 1963. Statistics of meteor streams. Smithsonian Contributions to Astrophysics 7, 261.

Toth, J. an Piffl, R., Koukal, J., Zoladek, P., Wisniewski, M., Gajdos, S., Zanotti, F., Valeri, D., De Maria, P., Popek, M., Gorkova, S., Vilagi, J., Kornos, L., Kalmancok, D., Zigo, P., 2012. Video observation of Draconids 2011 from Italy. WGN, Journal of the International Meteor Organization 40, 117–121.

Trigo-Rodríguez, J.M., Madiedo, J.M., Williams, I.P., Dergham, J., Cortés, J., Castro-Tirado, A.J., Ortiz, J.L., Zamorano, J., Ocaña, F., Izquierdo, J., Sánchez de Miguel, A., Alonso-Azcárate, J., Rodríguez, D., Tapia, M., Pujols, P., Lacruz, J., Pruneda, F., Oliva, A., Pastor Erades, J., Francisco Marín, A., 2013. The 2011 October Draconids outburst — I. Orbital elements, meteoroid fluxes and 21P/Giacobini-Zinner delivered mass to Earth. In: Monthly Notices of the RAS 433, pp. 560–570. https://doi.org/10.1093/mnras/stt749. arXiv:1304.7635.

Vaubaillon, J., Colas, F., Jorda, L., 2005. A new method to predict meteor showers. I. Description of the model. Astron. Astrophys. 439, 751–760. https://doi.org/10.1051/0004-6361:20041544.

Vaubaillon, J., Watanabe, J., Sato, M., Horii, S., Koten, P., 2011. The coming 2011 Draconids meteor shower. WGN. Journal of the International Meteor Organization 39, 59–63.

Vokrouhlický, D., Farinella, P., 2000. Efficient delivery of meteorites to the Earth from a wide range of asteroid parent bodies. Nature 407, 606–608. https://doi.org/10.1038/35036528.

Watanabe, J.I., Sato, M., 2008. Activities of parent comets and related meteor showers. Earth Moon and Planets 102, 111–116. https://doi.org/10.1007/s11038-007-9193-z.

Watanabe, J.i., Abe, S., Takanashi, M., Hashimoto, T., Iiyama, O., Ishibashi, Y., Morishige, K., Yokogawa, S., 1999. HD TV observation of the strong activity of the Giacobinid meteor shower in 1998. Geophys. Res. Lett. 26, 1117–1120. https://doi.org/10.1029/1999GL900195.

Watson Jr., F., 1934. Luminosity function of the Giacobinid meteors. Harvard College Observatory Bulletin 895, 9–16.

Whipple, F.L., 1951. A comet model. II. Physical relations for comets and meteors. Astrophys. J. 113, 464. https://doi.org/10.1086/145416.

Wu, Z., Williams, I.P., 1995. P/Giacobini-Zinner. Planetary and Space Science 43, 723–731.

Ye, Q., Wiegert, P.A., Brown, P.G., Campbell-Brown, M.D., Weryk, R.J., 2014. The unexpected 2012 Draconid meteor storm. Mon. Not. R. Astron. Soc. 437, 3812–3823. https://doi.org/10.1093/mnras/stt2178. arXiv:1311.1733.

Yeomans, D.K., 1971. Nongravitational forces affecting the motions of periodic comets Giacobini-Ziner and Borrelly. Astron. J. 76, 83. https://doi.org/10.1086/111089.

Yeomans, D.K., 1972. Nongravitational forces and periodic comet Giacobini-Zinner, in: The Motion, Evolution of Orbits, and Origin of Comets.

Yeomans, D.K., 1986. Physical Interpretations Form the Motions of Comets Halley and Giacobini-Zinner. (20th ESLAB Symposium).

Yeomans, D.K., Chodas, P.W., 1989. An asymmetric outgassing model for cometary nongravitationnal accelerations. Astron. J. 98, 1083–1093.